



**Developments in Laser-Based Diagnostics
for Wind Tunnels in the Aeromechanics
Division: 1987-1992**

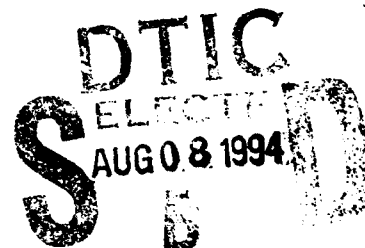
Linda G. Smith
Mark S. Maurice, PhD
Charles Tyler
John D. Schmisser
George L. Seibert, PhD
C. Dean Miller

May 1994

Final Report for Period January 1987 to December 1992.

10795

94-24896



Approved for public release; distribution is unlimited

FLIGHT DYNAMICS DIRECTORATE
WRIGHT LABORATORY
AIR FORCE MATERIEL COMMAND
WRIGHT-PATTERSON AIR FORCE BASE, OHIO 45433-7562

DTIC QUALITY INSPECTED 8

94 05 089

NOTICE

When Government drawings, specifications, or other data are used for any purpose other than in connection with a definitely Government-related procurement, the United States Government incurs no responsibility or any obligation whatsoever. The fact that the government may have formulated or in any way supplied the said drawings, specifications, or other data, is not to be regarded by implication, or otherwise in any manner construed, as licensing the holder, or any other person or corporation; or as conveying any rights or permission to manufacture, use, or sell any patented invention that may in any way be related thereto.

This report is releasable to the National Technical Information Service (NTIS). At NTIS, it will be available to the general public, including foreign nationals.

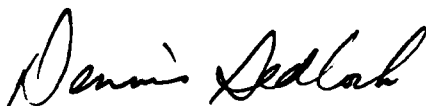
This technical report has been reviewed and is approved for publication.



LINDA G. SMITH
Aerospace Engineer
Experimental Facilities Research Branch



GEORGE L. SEIBERT, Chief
Experimental Facilities Research Branch
Aeromechanics Division



DENNIS SEDLOCK, Chief
Aeromechanics Division
Flight Dynamics Directorate

If your address has changed, if you wish to be removed from our mailing list, or if the addressee is not longer employed by your organization please notify WL/FIME, WPAFB, OH 45433-7005 to help us maintain a current mailing list.

Copies of this report should not be returned unless return is required by security considerations, contractual obligations, or notice on a specific document.

REPORT DOCUMENTATION PAGEForm Approved
OMB No. 0704-0188

Public reporting burden for this collection of information is estimated to average 1 hour per response, including the time for reviewing instructions, searching existing data sources, gathering and maintaining the data needed, and completing and reviewing the collection of information. Send comments regarding this burden estimate or any other aspect of this collection of information, including suggestions for reducing this burden, to Washington Headquarters Services, Directorate for Information Operations and Reports, 1215 Jefferson Davis Highway, Suite 1204, Arlington, VA 22202-4302, and to the Office of Management and Budget, Paperwork Reduction Project (0704-0188), Washington, DC 20503.

1. AGENCY USE ONLY (Leave blank)		2. REPORT DATE May 1994	3. REPORT TYPE AND DATES COVERED Final: Jan 87 to Dec 92	
4. TITLE AND SUBTITLE Developments in Laser-Based Diagnostics for Wind Tunnels in the Aeromechanics Division: 1987-1992			5. FUNDING NUMBERS PE-62201F PR-2404 TA-13 WU-21	
6. AUTHOR(S) Linda G. Smith, Dr. Mark S. Maurice, Charles Tyler John D. Schmisser, Dr. George L. Seibert, C. Dean Miller				
7. PERFORMING ORGANIZATION NAME(S) AND ADDRESS(ES) Flight Dynamics Directorate Wright Laboratory Air Force Materiel Command WPAFB OH 45433-7562			8. PERFORMING ORGANIZATION REPORT NUMBER	
9. SPONSORING/MONITORING AGENCY NAME(S) AND ADDRESS(ES) Flight Dynamics Directorate Wright Laboratory Air Force Materiel Command WPAFB OH 45433-7562			10. SPONSORING/MONITORING AGENCY REPORT NUMBER WL-TR-94-3054	
11. SUPPLEMENTARY NOTES				
12a. DISTRIBUTION/AVAILABILITY STATEMENT Approved for Public Release; Distribution in Unlimited.			12b. DISTRIBUTION CODE	
13. ABSTRACT (Maximum 200 words) The Aero-Diagnostics Research Section of the Aeromechanics Division develops and advances laser-based diagnostic techniques for use in a variety of subsonic through hypersonic wind tunnel facilities. These include laser velocimetry, laser induced fluorescence, Rayleigh scattering, phase shift holographic interferometry, and chemiluminescence. The purpose of this report is to bring the reader up to date on the status of these and other techniques under development in the Aeromechanics Division at the Wright Laboratory.				
14. SUBJECT TERMS Aerodynamic Measurements, Laser Velocimetry, Laser Induced Fluorescence, Chemiluminescence, Holographic Interferometry, Laser Light Sheet			15. NUMBER OF PAGES 106	
			16. PRICE CODE	
17. SECURITY CLASSIFICATION OF REPORT Unclassified	18. SECURITY CLASSIFICATION OF THIS PAGE Unclassified	19. SECURITY CLASSIFICATION OF ABSTRACT Unclassified	20. LIMITATION OF ABSTRACT Unlimited	

TABLE OF CONTENTS

LIST OF FIGURES	v
LIST OF TABLES	vii
PREFACE AND ACKNOWLEDGEMENTS	viii
1.0 INTRODUCTION	1
2.0 NOMENCLATURE	5
3.0 LASER VELOCIMETRY	8
3.1 THE LASER VELOCIMETRY (LV) MEASUREMENT TECHNIQUE	8
3.2 PRIMARY DIFFICULTIES IN HIGH SPEED FLOWS	12
3.3 RECENT ADVANCEMENTS IN THE STATE-OF-THE-ART	16
3.3.1 BOUNDARY LAYER MEASUREMENTS AT MACH 3 AND MACH 6	16
3.3.2 COMPRESSION RAMP AT MACH 6	21
3.3.3 SUPERSONIC VORTEX MEASUREMENTS AT MACH 1.9	25
3.3.4 EXPANSION FLOWS AT MACH 6	32
3.3.5 WEDGE FLOW AT MACH 3	35
3.3.6 INLET FLOW AT MACH 6	37
3.3.7 LV MEASUREMENTS AT MACH 12	40
3.4 REMAINING LIMITATIONS AND OUTLOOK	45
4.0 LASER INDUCED FLUORESCENCE AND RAYLEIGH SCATTERING	49
5.0 PHASE SHIFT HOLOGRAPHIC INTERFEROMETRY	59
6.0 CHEMILUMINESCENCE	71
7.0 OTHER TECHNIQUES	81

7.1 LASER LIGHT SHEET	81
7.2 COPPER VAPOR LIGHT SHEET	83
7.3 OPTICALLY SMART SURFACES	83
7.4 TOMOGRAPHY	85
7.5 MULTIPLE-SOURCE SCHLIEREN	86
8.0 CONCLUSIONS	88
9.0 REFERENCES	91

Accession For	
NTIS CRA&I	<input checked="" type="checkbox"/>
DTIC TAB	<input type="checkbox"/>
Unannounced	<input type="checkbox"/>
Justification	
By _____	
Distribution/_____	
Availability Codes	
Dist	Avail and/or Special
A-1	

LIST OF FIGURES

Fig. 1. Laser Velocimetry Concept	9
Fig. 2. Velocity Histogram	10
Fig. 3. Forward Scatter LV System Schematic	13
Fig. 4. Backward Scatter LV System Schematic	14
Fig. 5. Boundary Layer Profile on a Smooth Wall at Mach 3	18
Fig. 6. Boundary Layer Profile on a Rough Wall at Mach 3 for Various Reynolds Numbers	19
Fig. 7. Boundary Layer Surveys at Mach 6 on Rough and Smooth Plates	20
Fig. 8. Turbulence Intensities of Smooth Wall Boundary Layer at Mach 3	22
Fig. 9. Measured and Expected Shapes of the UV Cross Correlation Profiles on Smooth Wall at Mach 3	23
Fig. 10. Schematic of Supersonic Flow Over a Compression Ramp	24
Fig. 11. Velocity Histograms for Mach 6 Compression Ramp	26
Fig. 12. Schematic of Supersonic Vortex Flowfield on a Razor-Edged Delta Wing	28
Fig. 13. LV Measured Velocity Field for Supersonic Vortex	29
Fig. 14. Particle Trajectories in Mach 1.9 Vortex Flow	31
Fig. 15. Unseeded Regions on Ogive Cylinder and Flat Plate at Mach 6	33
Fig. 16. Velocity Histograms on Ogive Cylinder and Flat Plate at Mach 6	34
Fig. 17. Particle Size Calculation Through Oblique Shock Wave at Mach 3	36
Fig. 18. Boundary Layer Measured and "Corrected" Velocity Profiles on Wedge at Mach 3	38
Fig. 19. Velocity Profiles on P-8 Inlet at Mach 6	39

Fig. 20. Concept of Particle Size Distribution Calculations	41
Fig. 21. Particle Size Distribution in Inlet at Mach 6	42
Fig. 22. Measured, Corrected, and CFD Velocity Profiles in Inlet at $x = 20.27$ cm . . .	43
Fig. 23. Measured, Corrected, and CFD Velocity Profiles in Inlet at $x = 31.43$ cm . . .	44
Fig. 24. RMS and Mean Velocities Through Shear Layer at Mach 12	46
Fig. 25. Computed Trajectories for Alumina Particles through Nozzle Expansion	47
Fig. 26. Laser Induced Fluorescence System Schematic	50
Fig. 27. Density Distribution Measured as Model is Injected and Removed Repeatedly . .	53
Fig. 28. Density Distribution Measured as the Tunnel is Pumped Down to Vacuum	55
Fig. 29. Density Distribution Measured as the Tunnel is Vented to Atmospheric Pressure	56
Fig. 30. Density Distribution at Several Pressures	57
Fig. 31. y, z, r Coordinate System	62
Fig. 32. Phase Shift Holographic Interferometry Writer System	64
Fig. 33. Phase Shift Holographic Interferometry Reader System	65
Fig. 34. Schematic of Wedge and Flowfield	67
Fig. 35. Infinite Fringe Interferogram of Wedge at Mach 3	68
Fig. 36. Finite Fringe Interferogram of Wedge at Mach 3	69
Fig. 37. Shadowgram of Wedge at Mach 3	70
Fig. 38. Chemiluminescence System	73
Fig. 39. Spectrum of Absorption Coefficients for Molecular Oxygen	75
Fig. 40. Velocity Profile from Chemiluminescent Flow Visualization	78
Fig. 41. Example Flow Visualization of Shock Structure Using Chemiluminescence . . .	79

LIST OF TABLES

Table 1.	Tunnel Operating Conditions	4
Table 2.	Feasibility of Tomography in Facilities	85

PREFACE AND ACKNOWLEDGEMENTS

As the art and science of aeronautics has developed through this century, the demand for techniques to measure the critical flow parameters throughout the expanding flight envelope has continued to challenge the experimentalist. From the early days of the Wright brothers, who tested airfoil shapes on bicycles, to the modern era of large wind tunnels testing full scale aircraft, understanding, managing and predicting the movement of bodies through the viscous media on and above the Earth has continued to challenge each new generation of advocates.

Experimental test developers have attempted to keep pace with the "faster, higher, farther" visionaries by creating "visions" of their own - techniques that use the unique properties of light, particularly the coherence, monochromaticity and power of LASER light.

In the early 1980's, The Aeromechanics Division of the then Flight Dynamics Laboratory realized the need to centralize the division efforts in this area of nonintrusive diagnostics and they created the Aero-Optical Instrumentation Group. The Group mission was to conduct research and development programs to conceive, develop, test and transition new and improved nonintrusive, aeromechanic simulation techniques and test capabilities, integrate advanced diagnostic methods for experimental validation of computational fluid dynamics codes and develop and evaluate air-data sensor concepts.

Initial efforts centered on developing LASER Velocimeter (LV) and holographic interferometry (HI) techniques for use in the most accessible test facilities. Early programs focused on obtaining single component LV measurements in the Trisonic Gasdynamics Facility

(TGF) and two component measurements in the Vertical Wind Tunnel (VWT). Seeding the flow was (and remains to this day) one of the most critical aspects of LV studies and it was quickly determined that each facility required a unique approach to seeding. Resident expertise in HI allowed for some immediate work to be performed in the Mach 3 and Mach 6 High Reynolds Number facilities. This was followed by LV measurements in these facilities which required the development of a special high pressure seeder using silicon oil that could operate over a range of stagnation pressures to 2100 psi. With continued system development, LV measurements were made in all of the test facilities in the division, resulting in first ever velocity measurements at Mach 6 and Mach 12. Concurrent research led to the characterization of particle size based on particle drag forces through known aerodynamic phenomena (e.g., shock waves) and the subsequent determination of the correction for particle lag bias.

Simultaneously, Flow Visualization systems were developed to complement other measurement techniques and were used extensively to observe the physical behavior of flows around complex bodies, greatly contributing to the understanding of these flows. The results of all these activities significantly influenced the design of the Subsonic Aerodynamic Research Laboratory (SARL), resulting in a facility with more than 56% visibility in the test section, allowing for easy optical access.

Early in its development it was realized that LV techniques could not measure velocity fields in situations where the particles could not emulate the actual fluid flow. It was recognized that techniques were required that tracked the actual gas molecules using methods that probed the gas either elastically or inelastically. In the mid 80's, a concerted effort was made to begin development of systems that used spectroscopic techniques to measure temperature, pressure,

density and species concentration, among others. These systems are currently under development.

We wish to acknowledge the USAF contractors who have contributed to these efforts. The laser induced fluorescence and Rayleigh scattering system was designed by Dr. Anthony O'Keefe at Deacon Research Corp. Design of the phase shift interferometry system was accomplished by Charles Lysagorski of KMS Fusion. The chemiluminescence concept was developed by Dr. Morton Camac at Aerodyne Corporation. The optically smart surfaces are currently under development by Dr. James Trolinger and Dr. James Millerd of MetroLaser. These projects have been funded by the Small Business Innovative Research program.

The investigation of tomography for use in our wind tunnels is being conducted by Professor Soyoung Cha from the University of Illinois at Chicago. Professor Steven Collicott has conducted the evaluation of multiple-source schlieren for our facilities. Professors Cha and Collicott were sponsored by the Air Force Office of Scientific Research. Mr. Andrew Johnston, an AFOSR Summer Graduate Student, is credited with preliminary design of the test cell for the chemiluminescence system.

Finally, we thank the wind tunnel facility technicians and operators within the Aeromechanics Division.

1.0 INTRODUCTION

The Aero-Diagnostics Research Section of the Aeromechanics Division, Wright Laboratory develops advanced laser-based diagnostic systems for use in wind tunnel testing. Some of the techniques in use or under development by the section include laser velocimetry, laser induced fluorescence, Rayleigh scattering, phase shift holographic interferometry, and chemiluminescence. These techniques provide nonintrusive off-body measurements for flow structure analysis and computational fluid dynamics (CFD) code validation.

The achievements of computational fluid dynamics (CFD) towards flowfield analysis and vehicle design are well known. However, despite the tremendous advancements in CFD over the last decade, most solutions all flow regimes are still reliant on constitutive models of turbulence and boundary conditions. Consequently, experimental flowfield measurements are necessary for the development of these models and the validation of computational solutions. Mechanical probes can provide skin friction, pressure, and temperature measurements; however, the probes are intrusive and thus modify the flowfield being measured. On the other hand, nonintrusive techniques cause no such problems. The emphasis on nonintrusive or advanced laser-based diagnostic methods is spurring the development of the systems described in this report. The diagnostics under development will measure density, pressure, temperature, velocity, and surface strain.

One primary flowfield parameter is the velocity, for which quantitative, nonintrusive techniques generally fall into two categories: molecular and particle. Molecular techniques such

as electron beam (Ref. 1), planer laser induced fluorescence (PLIF) (Ref. 2), Rayleigh scattering (Ref. 3) and chemiluminescence (Ref. 4) are based on optical measurements of light detected from molecules or atoms within the flow. These techniques are promising; however, they have not yet evolved from the laboratory setting to complex, supersonic wind tunnel applications.

In the second category are particle based techniques, such as laser velocimetry (LV) (Ref. 5), particle image velocimetry (PIV) (Ref. 6) and Doppler global velocimetry (DGV) (Ref. 7). These methods measure the velocity of particles within the flow, which requires that the particle velocities accurately model the fluid velocities for the measurements to be directly treated as fluid velocities. This is a primary drawback with the particle based techniques; however, in the case of LV, recent advancements in the ability to acquire measurements and analyze data, including particle dynamics, in the supersonic regime have kept this technique at the forefront of instrumentation capability for providing this data.

Laser Velocimetry (LV) is often utilized as an off-the-shelf nonintrusive measurement technique for low speed, steady state flows. However, in complex, supersonic flows, the application of LV becomes highly specialized. Set-ups must often contend with limited optical access, poor signal-to-noise ratios, and limited tunnel run times. Furthermore, seed particles must survive large ranges of flow temperatures and pressures, and extensive data analysis and interpretation are required to ascertain whether measured particle velocities are representative of the fluid flow. Several examples of LV studies in the supersonic regime demonstrate recent advancements and the current state-of-the-art of this measurement technique. Results are included from three wind tunnel facilities, operating at freestream Mach numbers of 1.9, 3, and 6, and track an evolution of applications from flat plate boundary layers to the complex flowfield of a

supersonic inlet. Results demonstrate that further development of collection, seeding and analysis techniques will continue to extend the range of LV applications and measurement statistics, but the overall limiting factor will continue to be the ability of LV seed to model the discrete motion of fluid molecules.

A description of the LV technique and the complications of applying LV in supersonic flows is followed by a presentation of each test in terms of its individual contributions towards extending the state-of-the-art. From this chronology it is clear that much more information is contained within LV data than can yet be deciphered; however advancements in the ability to measure seeded flows will not eliminate the need for continued development of the molecular based techniques. In the interest of space, only synopses of these tests are given and the reader should refer to the references for further detail.

Following the laser velocimetry section, the developments and advances of the technologies for laser induced fluorescence (LIF), Rayleigh scattering, phase shift holographic interferometry, and chemiluminescence are discussed. The other techniques in use or under development include laser light sheet, copper vapor light sheet, optically smart surfaces, tomography, and multiple-source schlieren.

The wind tunnels currently in use in the Aeromechanics Division include the Subsonic Aerodynamic Research Laboratory (SARL), Trisonic Gasdynamics Facility (TGF), Mach 3 and Mach 6 High Reynolds Number Facilities (Mach 3 HRNF and Mach 6 HRNF), 20-inch Mach 12/14 Hypersonic Wind Tunnel (HWT), and a Large Water Tunnel (LWT). The diagnostic

techniques will be linked with the facilities for which they are being developed in the body of this paper. Tunnel operating Mach and Reynolds numbers are shown in Table I.

Table 1. Tunnel Operating Conditions

Facility	Mach Number	Reynolds Number
SARL	0.1 - 0.6	$< 10.8 \times 10^6/\text{m}$
TGF (subsonic)	0.23 - 0.85	$< 8.2 \times 10^6/\text{m}$
TGF (transonic)	0.3 - 1.0	$< 26.2 \times 10^6/\text{m}$
TGF (supersonic)	1.5, 1.9, 2.3, 3.0	$9.8 \text{ to } 16.4 \times 10^6/\text{m}$
Mach 3 HRNF	3.0	$32.8 - 328 \times 10^6/\text{m}$
Mach 6 HRNF	5.76	$4.9 - 98.4 \times 10^6/\text{m}$
HWT	12.0, 14.0	$1.3 - 3.28 \times 10^6/\text{m}$
Large water tunnel	0.046 - 0.26 m/sec	

2.0 NOMENCLATURE

c	Constant in Eq. (29)
C_d	Drag coefficient defined by Eq. (9)
C_{d1}	Function defined by Eq. (10)
d	Particle diameter
f	Function defined by Eq. (21)
g	Function defined by Eq. (11)
h	Function defined by Eq. (12)
h	Planck's constant
I	Intensity
I_0	Background intensity
I_i	Phase shifted intensity values, $i = 1, 2, 3$
k	Intensity rate constant, Eq. (26)
k_1	Constant, Eq. (27)
K_m	Chemiluminescence rate constant, Eq. (28)
K	Gladstone-Dale constant, Eq. (18)
L	Optical pathlength through test section
M	Mach number
n	Number of individual measurements
n	Number density in chemiluminescence
n	Index of refraction in interferometry
P	Pressure

r	Radial coordinate
R	Radius of field
Re	Reynolds number
T	Temperature
T	Time as used in Eq. (28-30)
u, U	Velocity component in x-direction
\bar{u}	Mean velocity in x-direction
u'	Velocity fluctuation in x-direction
v	Velocity component in y-direction
V	Velocity vector
v'	Velocity fluctuation in y-direction
W	Function defined by Eq. (8)
x, y, z	Cartesian coordinate directions
$[NO]$	Concentration of NO

Greek

α	Angle-of-attack
δ	Boundary-layer thickness (99% U_∞)
σ	Standard deviation
γ	Modulation
γ	Ratio of specific heats
λ	Wavelength of laser
ν	Frequency of radiation
ρ	Density

ϕ Phase

Subscripts

AXIAL Axial direction

eff Effective

f Fluid property

i Summation index

L Maximum chord length of delta wing

msr Measured

N Normal

OUTER Outer edge of boundary layer

p Particle property

R The relative difference between the particle and the fluid

ref Reference

SHOCK Relative to shock orientation

T Tangential direction

VERTICAL Vertical direction

WEDGE Relative to wedge

x x-direction

0 Reference state

∞ Freestream

3.0 LASER VELOCIMETRY

3.1 THE LASER VELOCIMETRY (LV) MEASUREMENT TECHNIQUE

In order to understand the unique challenges of LV in the supersonic regime, it is necessary to understand the basic concepts of how a laser velocimeter works, the range of measurement statistics which can be calculated, and how an LV system is configured in relation to the wind tunnel.

The basic principle of LV is shown schematically in Fig. 1. At the intersection of two monochromatic, coherent laser beams an optical probe volume is formed which consists of a series of parallel interference fringes. As a "seed" particle within the flow passes through this probe volume, the intensity of the scattered light varies sinusoidally with a frequency that is directly proportional to the particle velocity in the direction normal to the fringes. This light is collected by a photomultiplier tube (PMT), converted to an electronic signal, and then analyzed to produce a single velocity measurement. Simultaneous multiple velocity components are measured by forming cospatial probe volumes of different wavelengths of laser light and different orientations of fringes. Collected light is then separated into its constitutive wavelengths and each component is processed independently.

At each flowfield location, many individual velocity measurements are collected. Shown in Fig. 2 is a velocity histogram of 1500 individual measurements in the freestream of a Mach 3 tunnel. The general distribution has a Gaussian shape with a mean velocity of 541 m/s and a standard deviation of 14.0 m/s, calculated as:

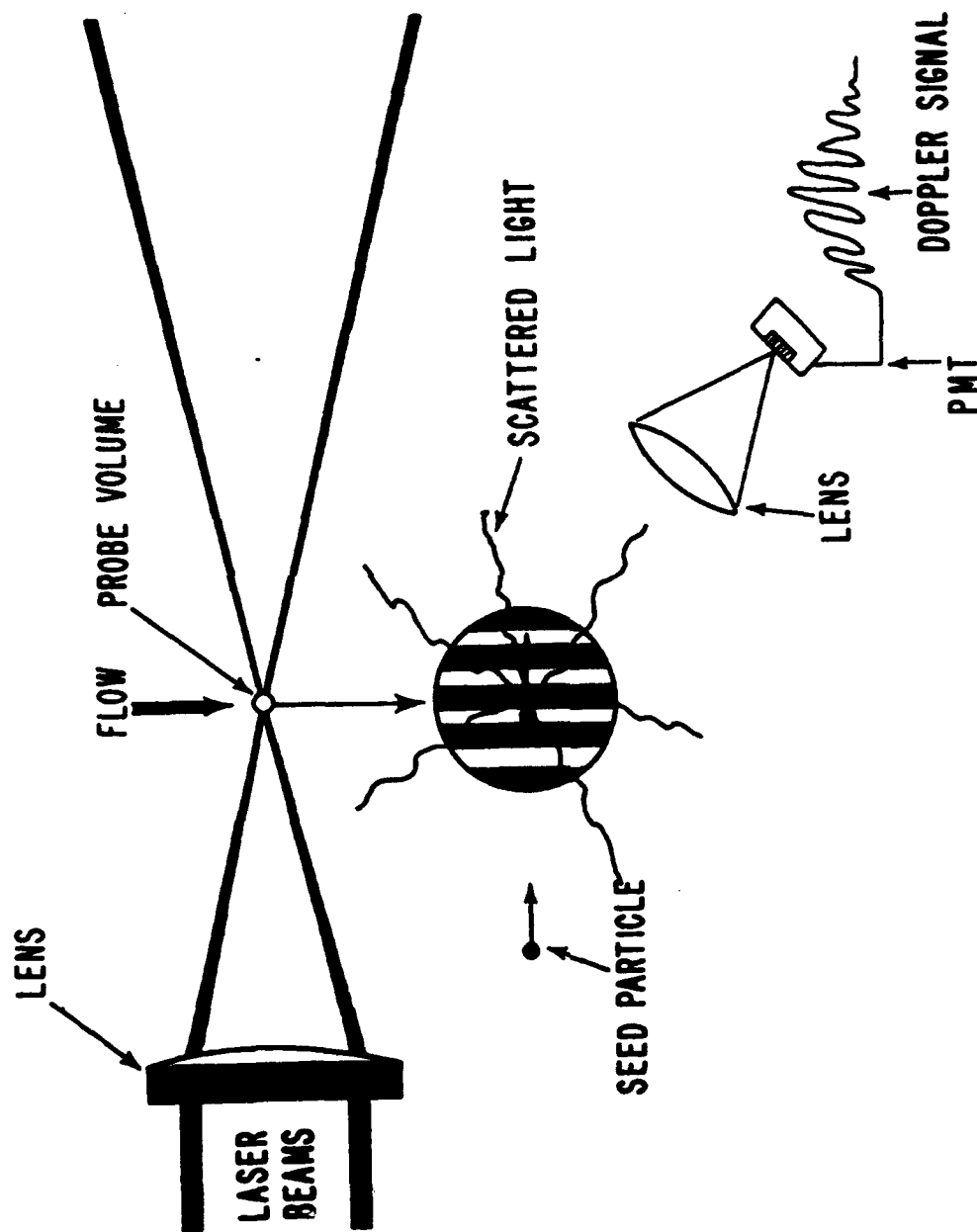


Fig. 1. Laser Velocimetry Concept.

VELOCITY HISTOGRAM

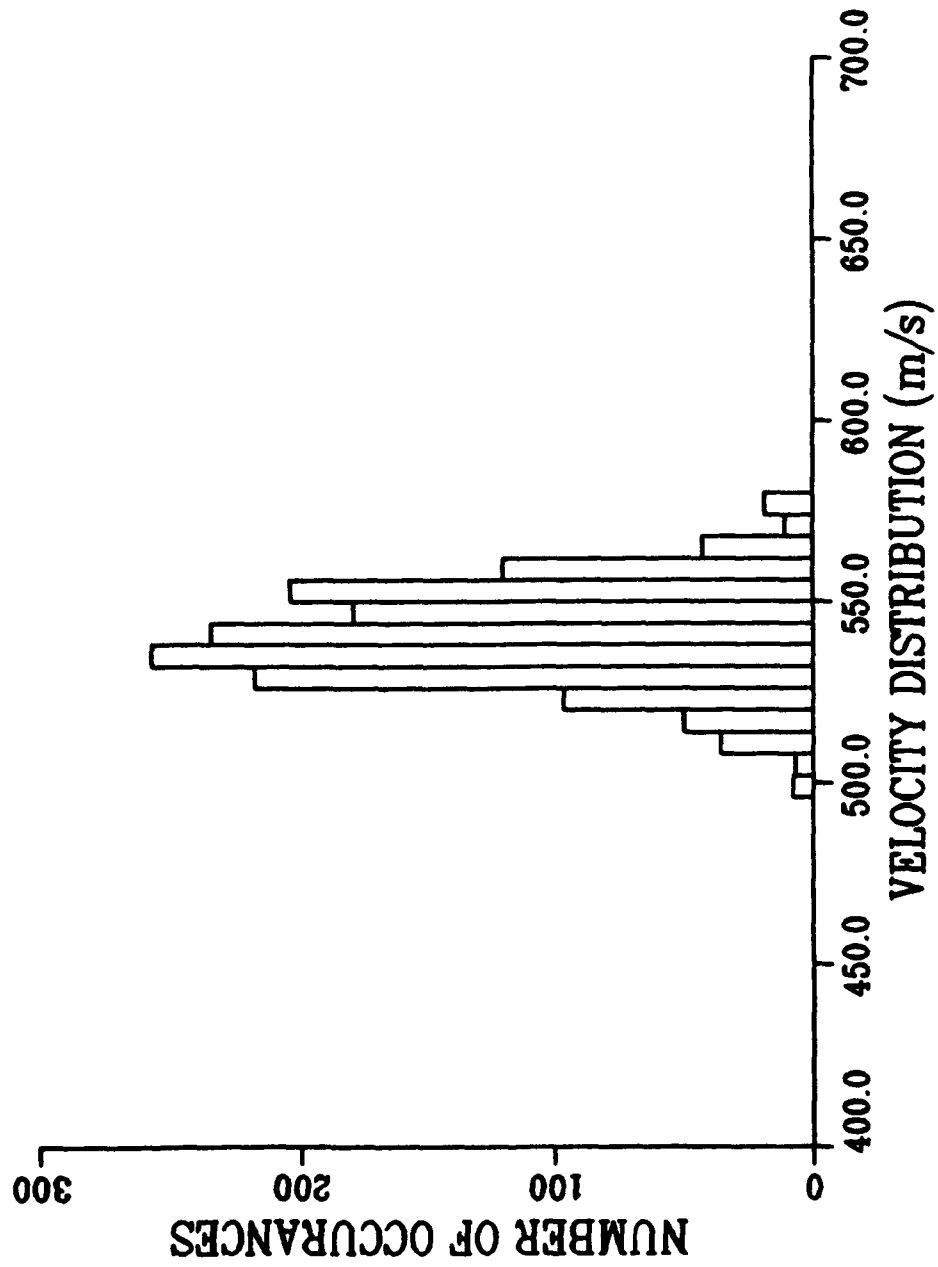


Fig. 2. Velocity Histogram.

$$\bar{u} = \frac{1}{n} \sum_{i=1}^n u_i \quad (1)$$

and

$$\sigma = \left[\frac{1}{n} \sum_{i=1}^n (u_i - \bar{u})^2 \right]^{1/2} \quad (2)$$

which corresponds to a turbulence intensity of 2.6%, defined as:

$$\% \text{ turbulence intensity} = \sigma / \bar{u} \times 100 \quad (3)$$

Higher order moments, which describe the histograms deviation from an ideal Gaussian curve, include its skewness of 0.06, calculated as:

$$\text{skewness} = \frac{1}{\sigma^3} \frac{1}{n} \sum_{i=1}^n (u_i - \bar{u})^3 \quad (4)$$

and its flatness, or kurtosis, of 2.93, calculated as:

$$\text{kurtosis} = \frac{1}{\sigma^4} \frac{1}{n} \sum_{i=1}^n (u_i - \bar{u})^4 \quad (5)$$

For an ideal Gaussian distribution the skewness is zero and the kurtosis is three.

For multiple velocity components, a wealth of correlation statistics can also be calculated, such as:

$$\overline{u'v'} = \frac{1}{n} \sum_{i=1}^n (u_i - \bar{u})(v_i - \bar{v}) \quad (6)$$

which is a primary term in calculating Reynolds stress.

For most supersonic wind tunnel applications, LV systems are used in either forward scatter or backward scatter configurations. In forward scatter, shown in Fig. 3, the transmission and collection optics are positioned on opposite sides of the test section, requiring two traverse systems which must track each other accurately for the collection optics to maintain focus on the probe volume. In backward scatter, shown in Fig. 4, the scattered light is collected through the same window that transmits the laser beams. In this case only one traverse is required; however, the intensity of the scattered light in this direction is nominally 1/100 of that seen in forward scatter. Therefore, although a forward scatter configuration is much more complicated to work with, it is often necessary to achieve the signal quality and intensity required by LV processors.

3.2 PRIMARY DIFFICULTIES IN HIGH SPEED FLOWS

There are several reasons why the use of LV in supersonic flows tends to be much more difficult than for low speed applications. For example, optical access is generally more limited, which constrains beam spacing, and the potential field of view for both transmission and collection optics. In addition, the focal length to the measurement location can be restricted both

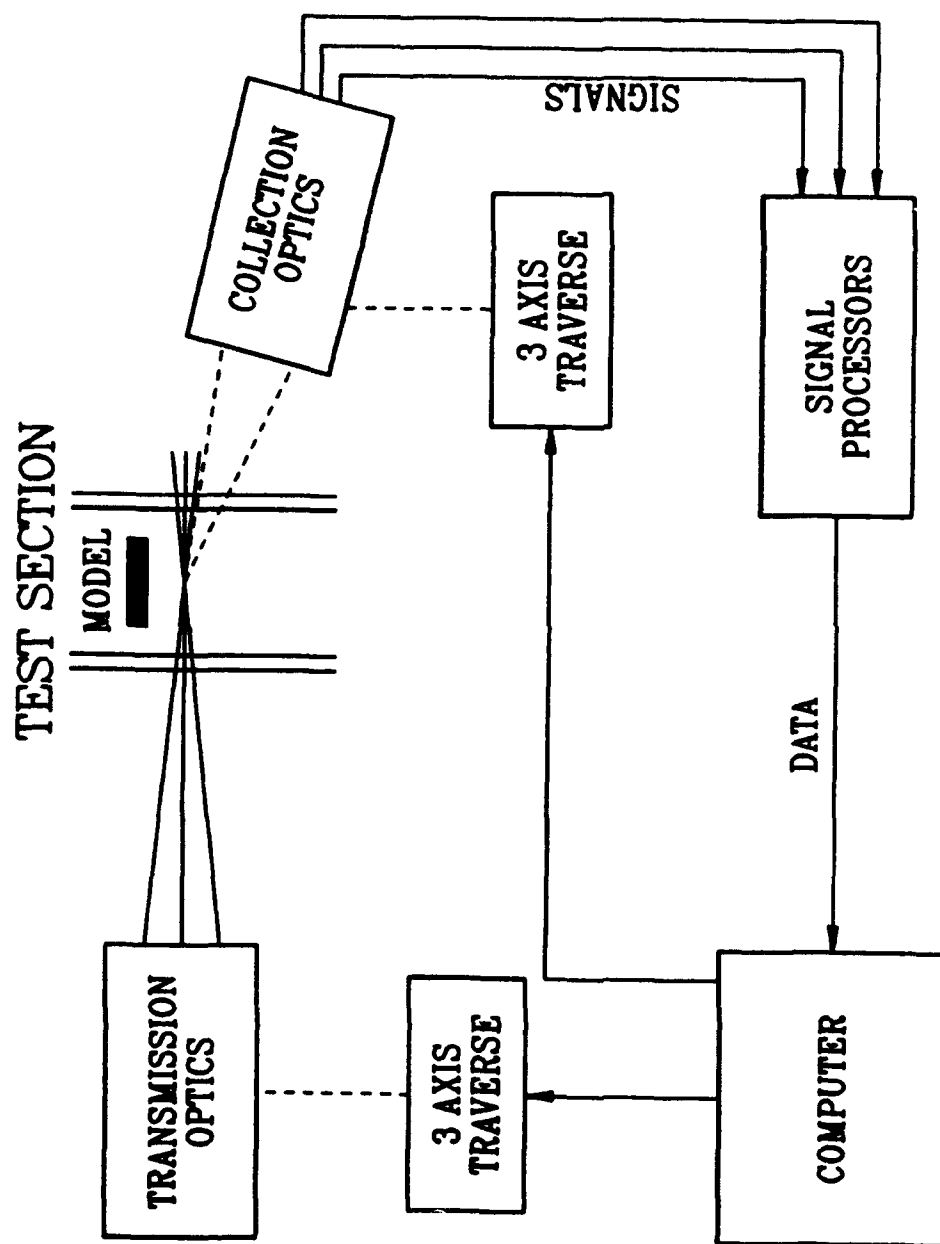


Fig. 3. Forward Scatter LV System Schematic.

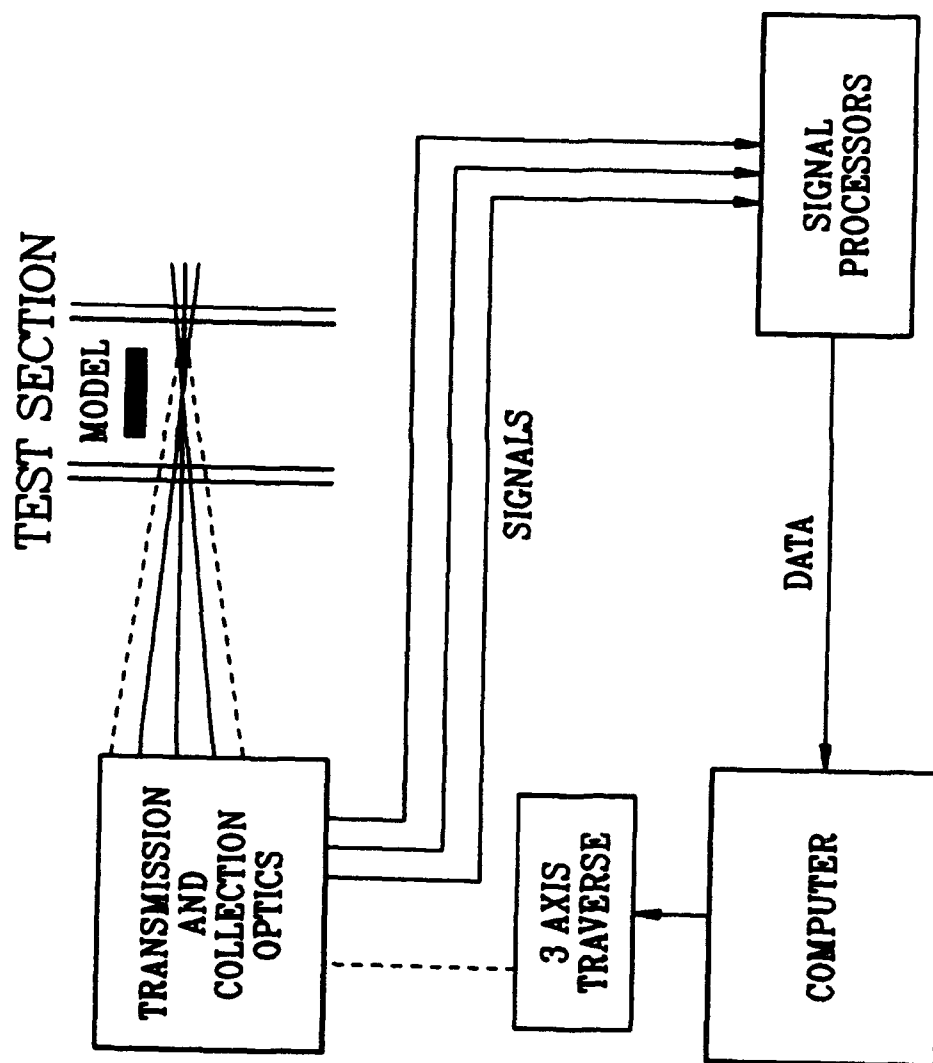


Fig. 4. Backward Scatter LV System Schematic.

by optical and physical access. Tunnel run times are often limited by air storage or heater capacity, and operation can be more expensive. Vibration can be more severe and heating can cause movement of the model as well as the entire tunnel. Limited access around the test section often requires that transmission and collection optics be on separate traverse systems. If, for example, the traverses are required to track within 0.02 mm over a 15 cm distance, the two systems must be aligned parallel to within 0.008° of each other. High velocities limit how small the probe volume can be made since a smaller volume corresponds to higher frequencies, and all LV processes are limited in frequency range. In turn, a larger probe volume means poorer spatial resolution and reduced light intensity.

Another difficulty in high speed flows is the selection and introduction of a suitable seed material. In general, the selection of LV seed is based on a variety of considerations (Ref. 8), including scattering characteristics, interaction with model and tunnel components, toxicity, number concentration, size, and density. Optically, the seed must scatter sufficient light to differentiate the particle velocity from background noise. Aerodynamically, the particles must be as small and light as possible in order to respond to the structure of the flow.

In low speed flows, accurate LV measurements can be obtained from a wide variety of seed materials. Solid particles and aerosols can be introduced into the flow using commercially available seeders, and particle size measurements can be collected simultaneously with the velocity (Ref. 9). In high speed flows these luxuries do not exist. Solid particles of measurable size, such as aluminum oxide or silicon oxide can be abrasive to model surfaces and respond poorly to flowfield gradients such as shockwaves, expansion waves, vortices and boundary layers. Less dense materials, such as polystyrene, do not survive the high stagnation

temperatures of heated flows, and in supersonic facilities with ambient stagnation temperatures carrier fluids such as alcohol do not completely evaporate (Ref. 10). Consequently, seeding within supersonic flows requires specially designed systems which often produce polydispersed particles of unknown size. And, as will be shown, the particles very often respond poorly to a variety of simple and complex flow structures.

3.3 RECENT ADVANCEMENTS IN THE STATE-OF-THE-ART

In recent years, several applications of LV in high speed flows have been performed at the Aeromechanics Division of the Wright Laboratory in order to extend the state-of-the-art in both the ability to collect LV measurements, and to apply the data towards quantitative flowfield analysis. The following test results demonstrate the evolution of these advancements and the challenges which remain.

3.3.1 BOUNDARY LAYER MEASUREMENTS AT MACH 3 AND MACH 6

In 1987 and 88, LV boundary layer profiles were obtained for both smooth and roughened surface flowfields at Mach 3 and Mach 6 (Ref. 11 and Ref. 12). The Mach 3 facility is a blowdown tunnel with a closed 20.3 x 20.3 cm test section. It uses unheated, compressed air and has a run time of approximately 5 to 10 minutes per day due to air storage limitations and refill time. Measurements were made along the tunnel centerline on the lower test section wall for Reynolds numbers from 48 to 350 million per meter.

The Mach 6 facility is also a blowdown tunnel and has similar run times; however, it uses heated air at 500-600 K and has an open jet test section with a 31 cm exit nozzle. Boundary layer profiles in this tunnel are at centerline stations along flat plates at zero degrees angle-of-attack for Reynolds numbers from 54 to 73 million per meter. Roughened surfaces for each case were machined 1.0 mm squares, 0.5 mm deep and spaced uniformly 1.0 mm apart.

A two-component LV system was used which consisted of an argon laser operating at 4 Watts, from which 514 nm green light and 488 nm blue light were used to measure the axial and vertical velocities. The system was configured in the forward scatter mode. The ellipsoidal probe volumes for each case were approximately 1.7 mm long spanwise across the tunnel with a centerline diameter of 0.328 mm. In each case, 1500 pairs of individual velocity samples were collected at each measurement location. The flows were seeded using silicon oil which was atomized and introduced into the stagnation chamber using a specially designed, high pressure seeder. (Ref. 38)

Results from these surveys are shown in Figs. 5 through 7. In both cases, the mean velocity profiles are smooth and repeatable, showing the effects of the roughness on the boundary layer development. In both cases, the mean velocity profiles are typical power law shapes. The smooth surface profile is much fuller, as would be expected, than the more developed profiles influenced by the surface roughness. For the rough wall profiles, the data does indicate the potential of a Reynolds number dependence, but the experimental accuracy is not high enough to confirm the trends shown or to validate this conclusion.

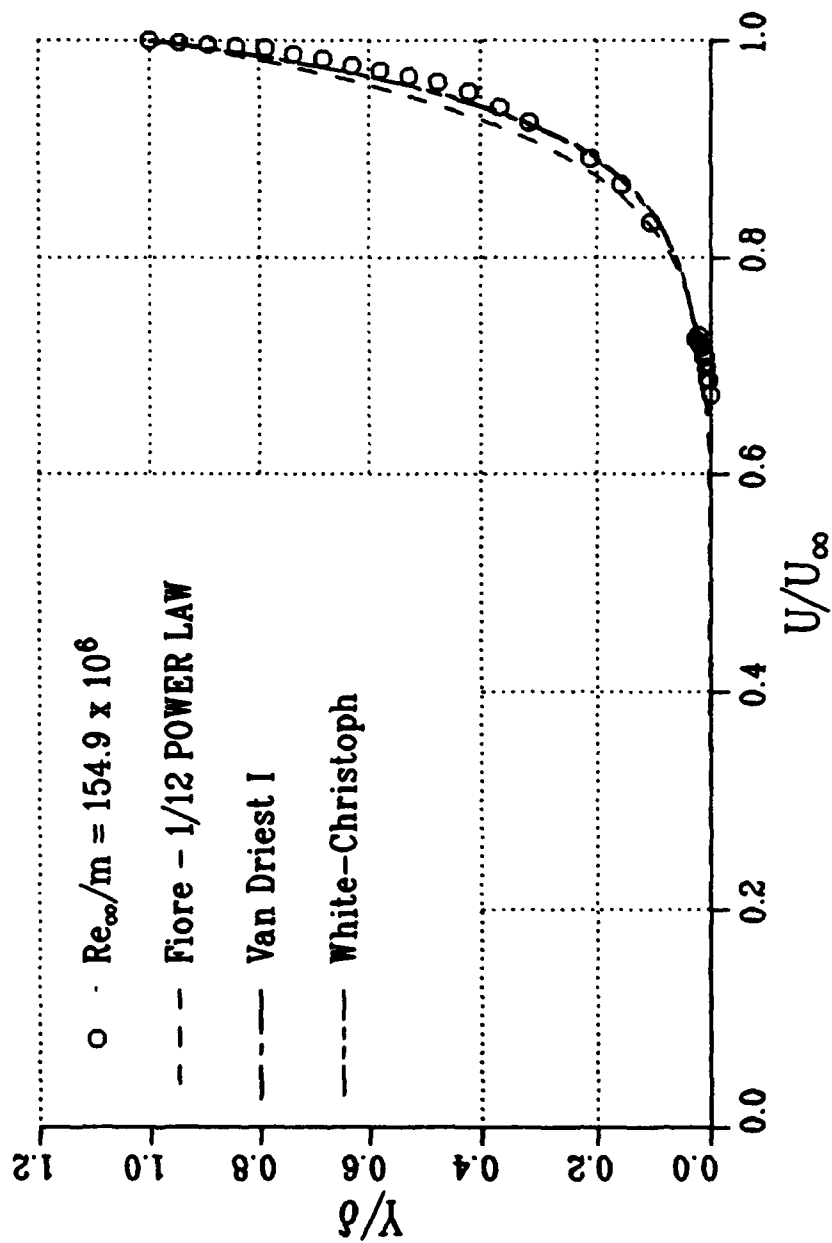


Fig. 5. Boundary Layer Profile on a Smooth Wall at Mach 3.

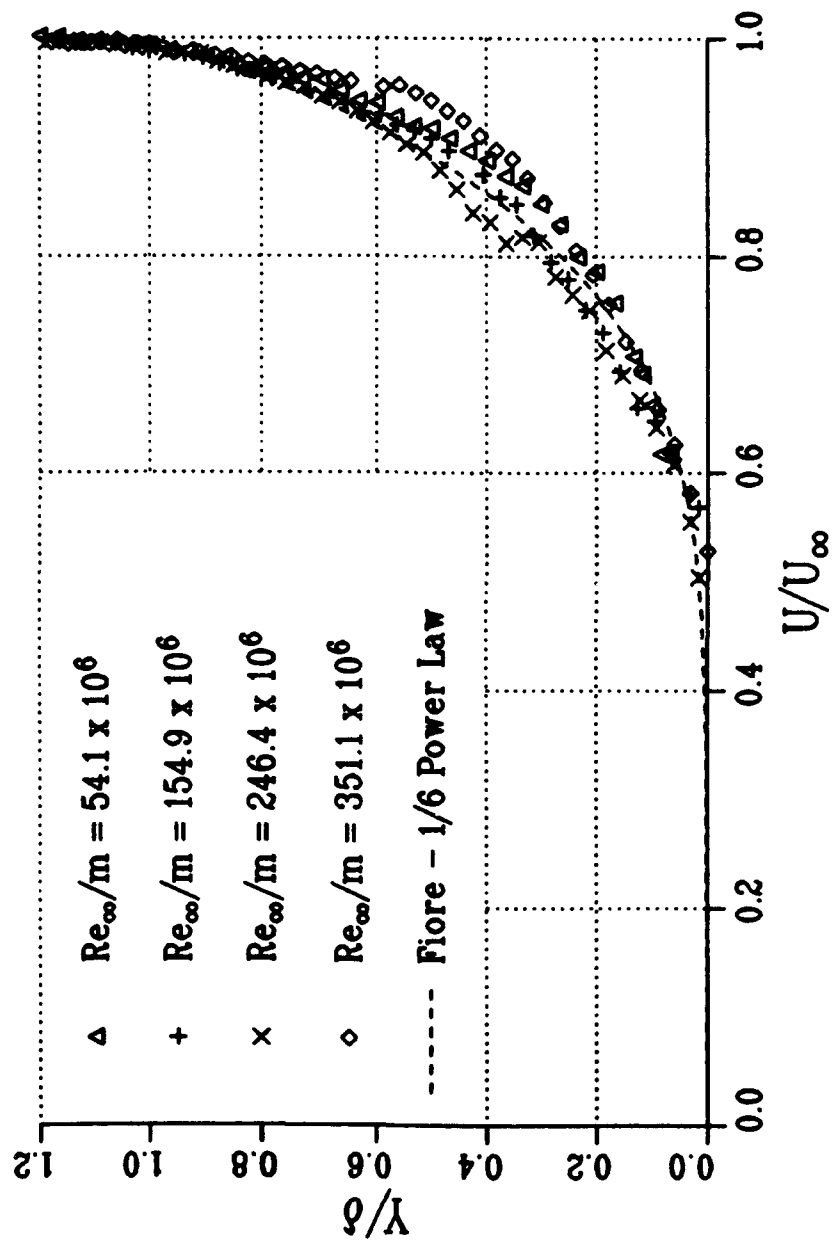


Fig. 6. Boundary Layer Profile on a Rough Wall at Mach 3 for Various Reynolds Numbers.

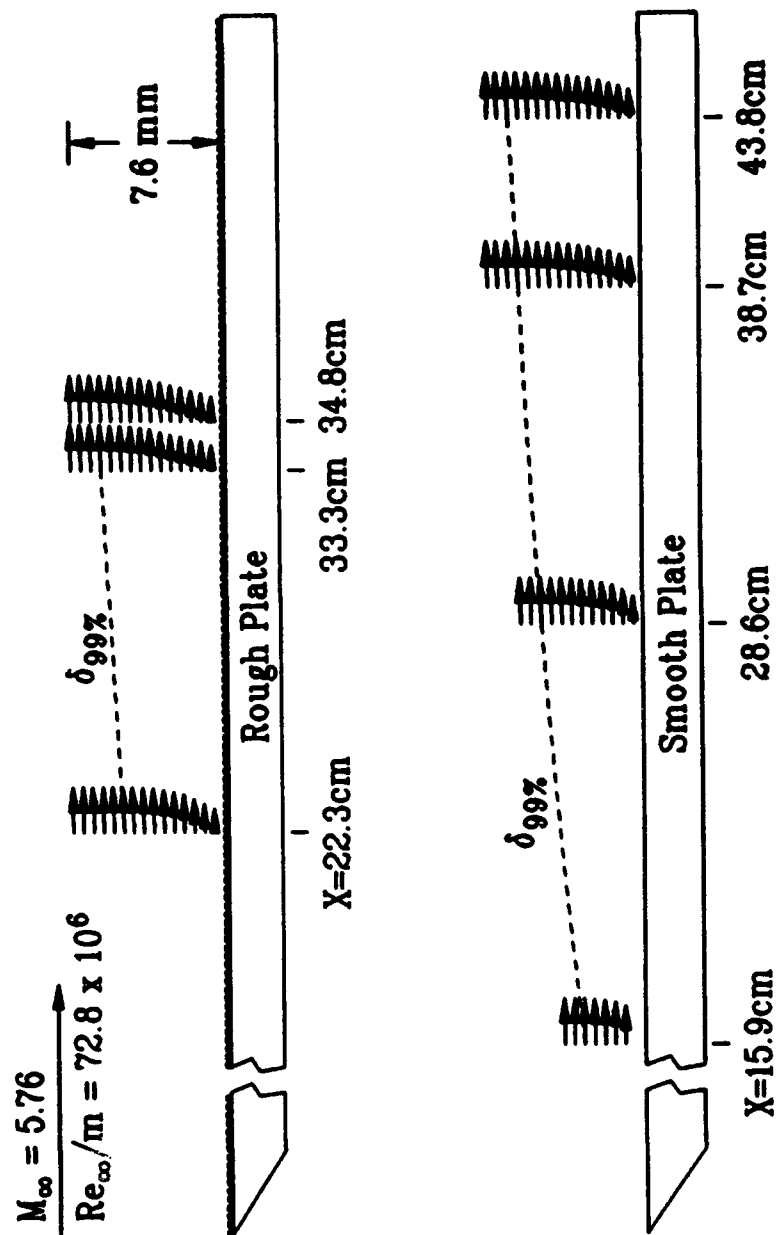


Fig. 7. Boundary Layer Surveys at Mach 6 on Rough and Smooth Plates.

The significance of these tests was in demonstrating the ability to acquire two-dimensional LV measurements in these environments, which required extreme precision in setting up the optical, mechanical and electronic components of the measurement system. These tests also demonstrated that the polydispersed silicon oil particles do not follow the turbulent structure within the flow. Turbulence intensity profiles are shown in Fig. 8 for a Mach 3 smooth wall survey. Both components show reasonable trends - a two percent freestream turbulence which remains relatively constant for the vertical component while the axial turbulence increases towards approximately 8 percent near the wall. However, the turbulence in the boundary layer is quantified by Reynolds stress, which is dominated by the cross correlation between the axial and vertical velocity fluctuations. This correlation is shown in Fig. 9. These experimental data compare poorly with the expected shape, and suggests that since the particles are not tracking the discrete motion of the turbulent eddies, the turbulence intensity statistics may be biased also.

3.3.2 COMPRESSION RAMP AT MACH 6

In addition to boundary layer measurements along the roughened flat plate in the Mach 6 facility, measurements were also obtained at the vertex and along the roughened surface of a 22 degree ramp which was installed onto the trailing edge of the plate (Ref. 12).

The purpose of this test was to obtain two-dimensional, supersonic LV measurements in a significantly complex flow which could not be adequately resolved by intrusive means. A detailed schematic of the flow over the ramp configuration is shown in Fig. 10. Due to the boundary layer interaction with the shock wave which turns the inviscid

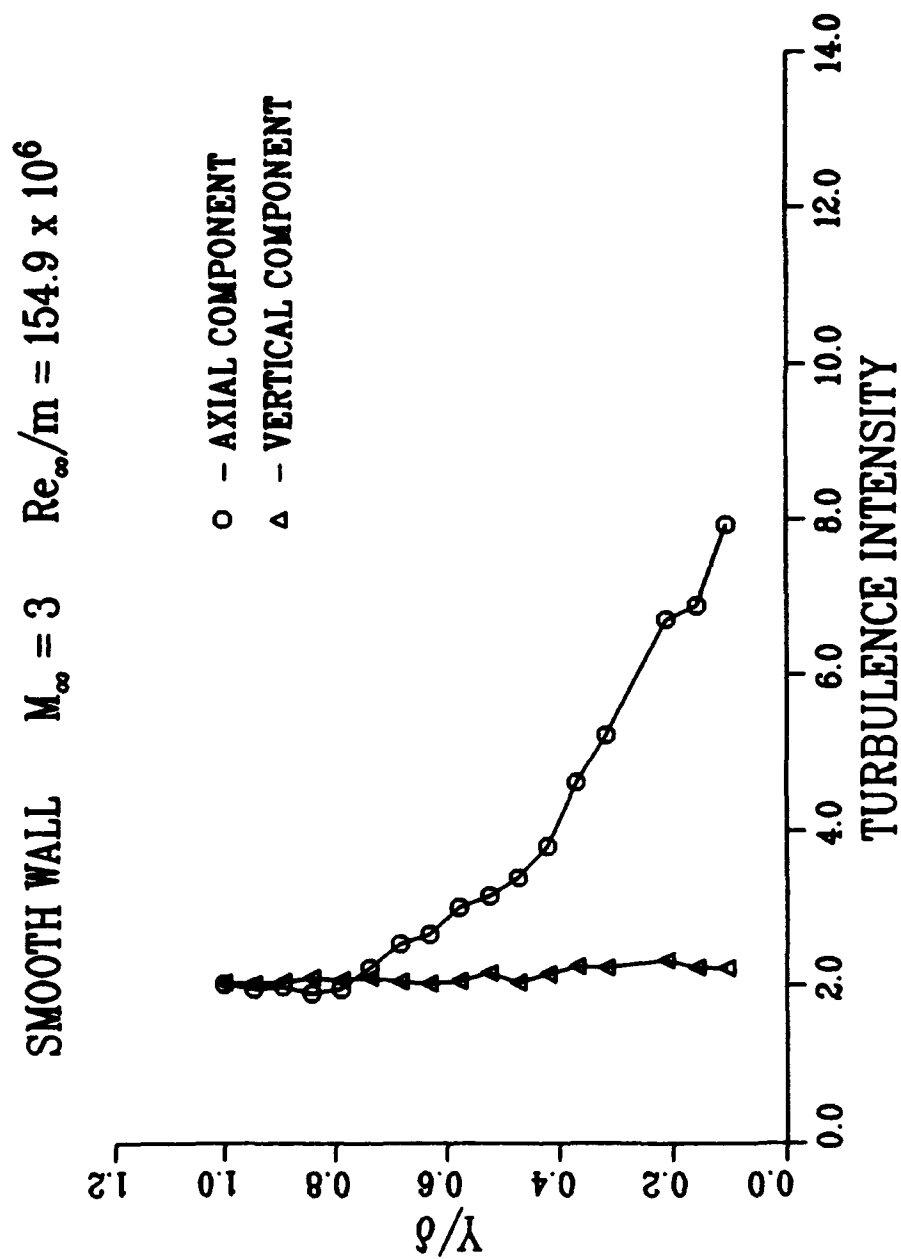


Fig. 8. Turbulence Intensities of Smooth Wall Boundary Layer at Mach 3.

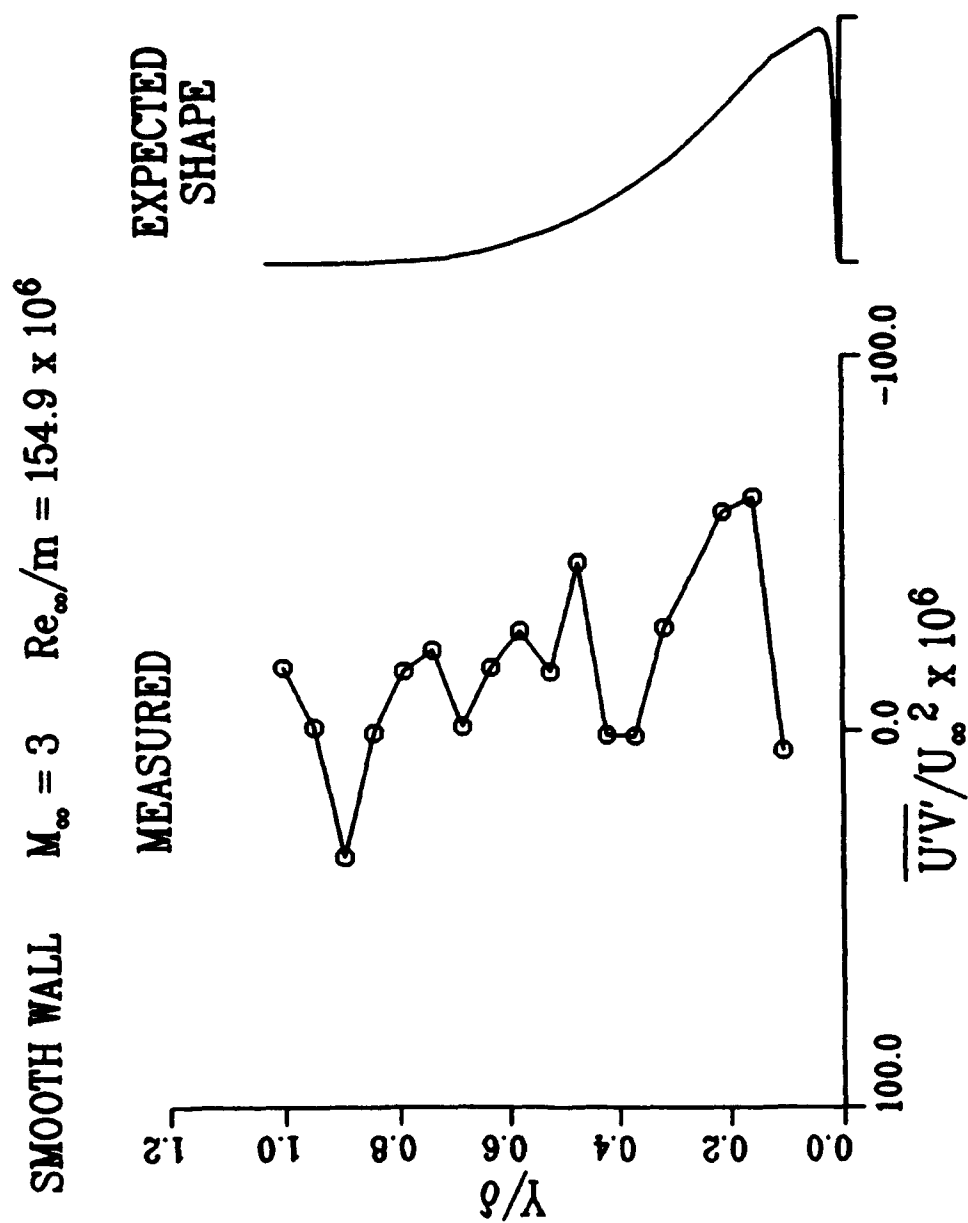


Fig. 9. Measured and Expected Shapes of the UV Cross Correlation Profiles on Smooth Wall at Mach 3.

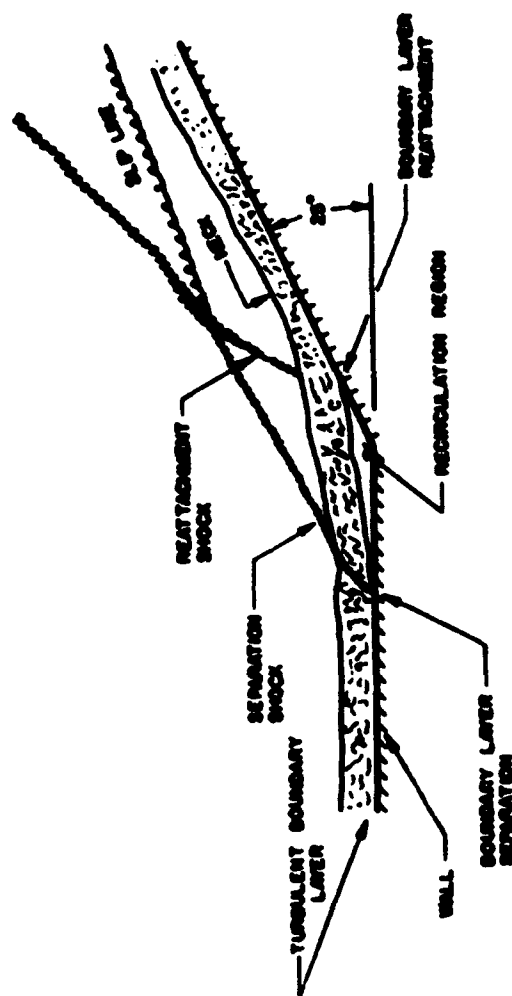


Fig. 10. Schematic of Supersonic Flow Over a Compression Ramp.

flow to run parallel with the ramp, the shock moves upstream of the vertex and causes the boundary layer to detach from the plate. The boundary layer reattaches to the ramp surface, leaving a very small separation bubble directly at the vertex. The measurement profiles in Fig. 11 represent data taken at freestream Reynolds numbers of 36.4 and 72.8 million per meter. Velocity histograms are shown due to the strong influence of particle dynamic bias within the data. Following the histograms from the freestream towards the plate, the outer measurement stations are above the separation shock, and show the high velocity and low turbulence intensity of the freestream. Just below the shock, only the smallest particles have relaxed to the fluid velocity, smearing the lower velocity distribution of the histogram. Continuing into the boundary layer, particles are further downstream of the shock. Consequently, there is a gradual shift within the histograms as different sized particles relax towards the fluid velocities at different rates.

Although the mean velocities and turbulence intensities from these histograms are highly biased, the quantitative trends within the data are clear, and a comparison between the two profiles shows that this flow structure is highly Reynolds number dependent.

3.3.3 SUPERSONIC VORTEX MEASUREMENTS AT MACH 1.9

The ability to obtain three component LV data in a complex supersonic flowfield was demonstrated for the vortical flow over a delta wing at Mach 1.9 (Ref. 13). These measurements were acquired in a closed circuit, continuous flow wind tunnel that operates at a Reynolds number up to 16.4 million per meter in the supersonic regime and has a 0.61 meter

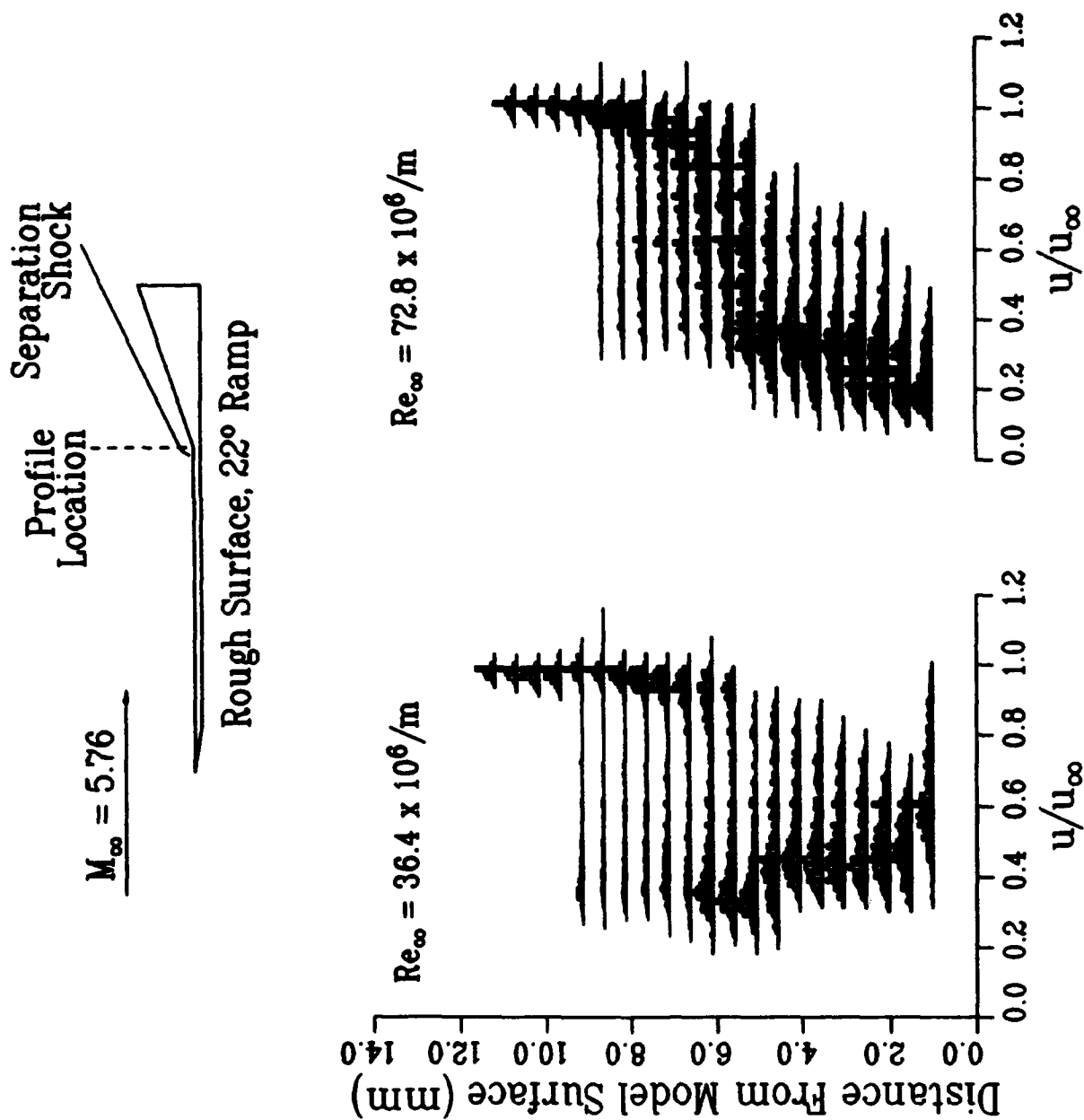


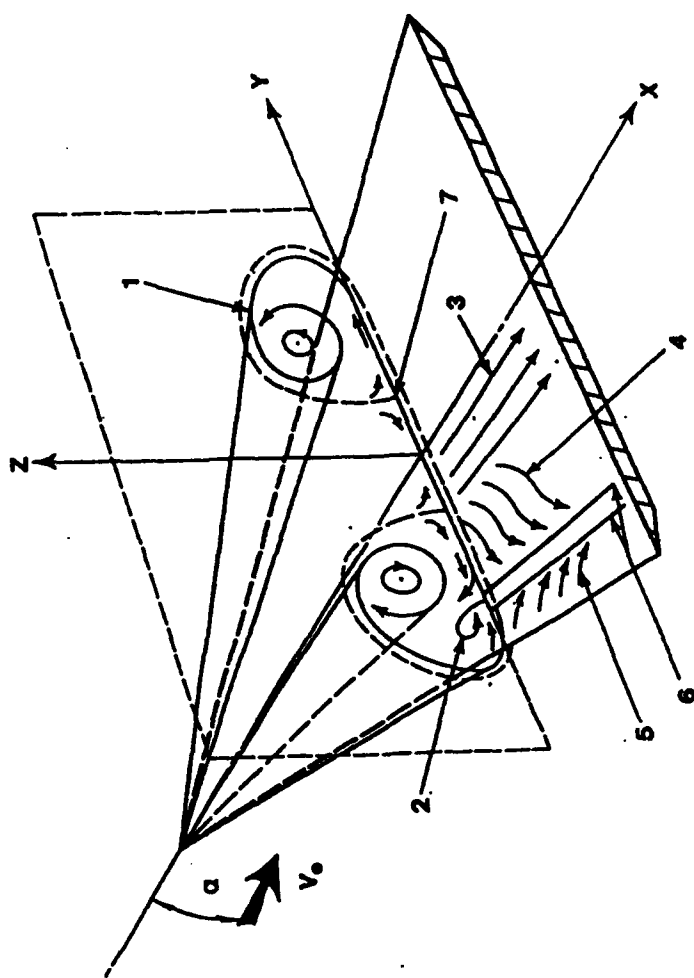
Fig. 11. Velocity Histograms for Mach 6 Compression Ramp.

square test section. The third component utilized the weaker 476 nm blue line from the argon laser.

The wind tunnel model was a simple 75° razor-edged delta wing that generates the vortical flowfield shown schematically in Fig. 12. Three velocity components in the primary vortex structure were measured on planes normal to the leeward surface at 40% and 80% chord for 20° and 30° angles-of-attack, and at 40% chord for 35° angle-of-attack. Shown in Fig. 13 is a velocity field for the 20° angle-of-attack, 80% chord survey. The void of data near the center of the vortex demonstrates that particle velocity lag is a dominant concern not only for turbulence measurements, but for mean velocities as well. Within the vortex, seed particles are centrifuged away from the core. Also, since larger particles are centrifuged more easily than smaller ones, the population density and size distribution of the seed varies radially through the field. A noted decrease in data rate toward the vortex core indicated the presence of fewer, smaller particles.

For this test it was demonstrated that the velocity lag bias could be predicted computationally (Ref. 14). A computational prediction (Ref. 15) for the flowfield was used in conjunction with a particle equation of motion of the form:

$$\begin{aligned} \frac{dV_p}{dt} = & \frac{-3C_d}{4d} \frac{\rho_f}{(\rho_p + \rho_f/2)} W|W| + \frac{\rho_f}{(\rho_p + \rho_f/2)} \frac{DV_f}{Dt} \\ & + \frac{\rho_f}{(\rho_p + \rho_f/2)} \frac{d}{dt} \left\{ V_f + \frac{d^2}{40} \nabla^2 V_f \right\} \end{aligned} \quad (7)$$



RAZOR-EDGED DELTA WING:

Chord Length: $c = 33.91$ cm

Span $[\odot x = c]: s = 18.17$ cm

SCHEMATIC FLOW DIAGRAM:

- 1] Scroll vortex sheet forming the main vortex
- 2] Secondary vortex
- 3] Central zone without vortex flows
- 4] Zone induced by the main vortex
- 5] Zone induced by the secondary vortex
- 6] Accumulation zone [air bubble or coating]
- 7] Reattachment lines

Fig. 12. Schematic of Supersonic Vortex Flowfield on a Razor-Edged Delta Wing.

LV MEASURED VELOCITY FIELD

$M = 1.9$
 $P_{\text{total}} = 57\,500 \text{ N/m}^2$
 $T_{\text{total}} = 311 \text{ K}$
 $x/L = 0.8$
 $\alpha = 20^\circ$

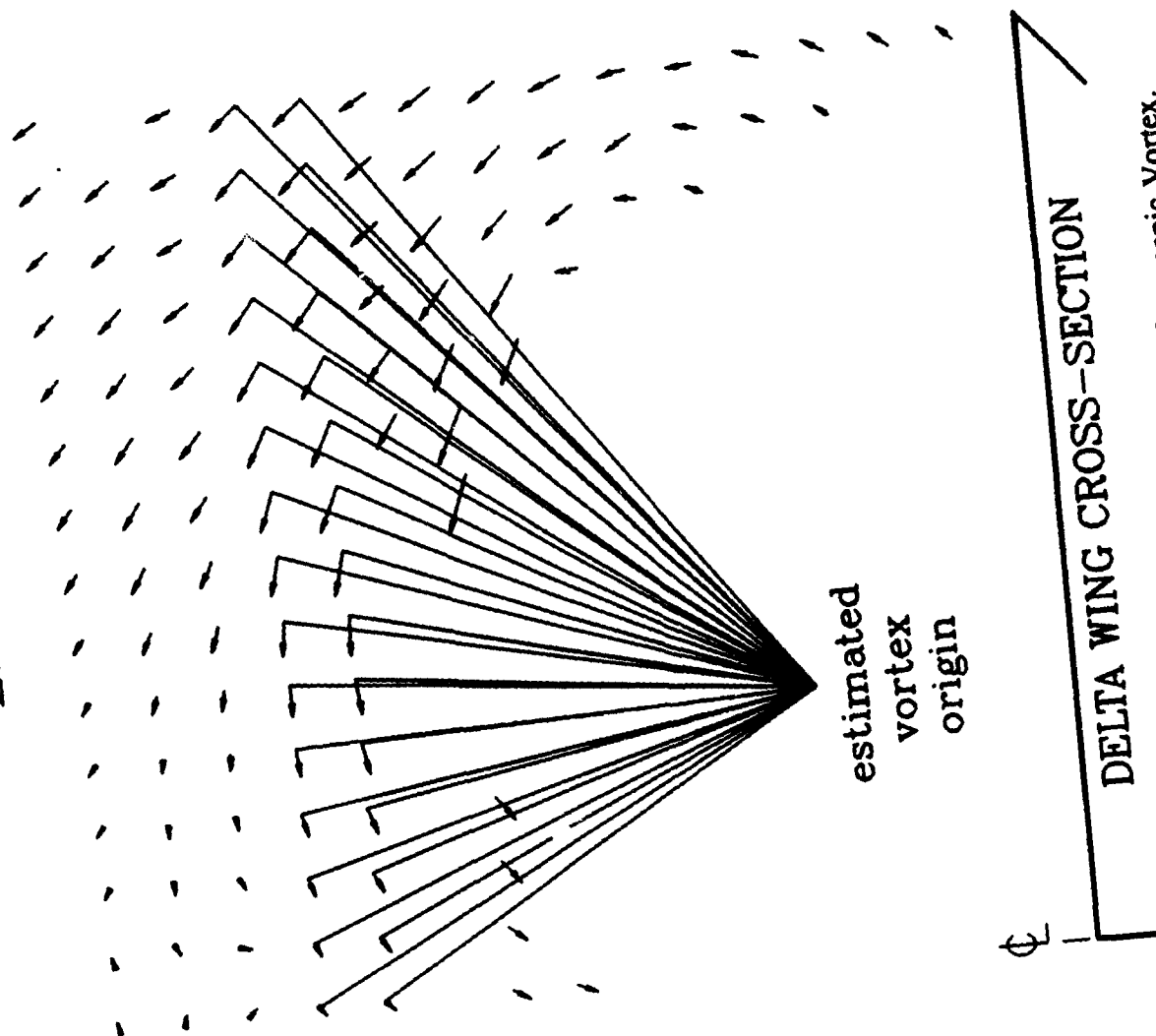


Fig. 13. LV Measured Velocity Field for Supersonic Vortex.

where:

$$W = V_p - V_f - \frac{d^2}{24} \nabla^2 V_f \quad (8)$$

with a drag law developed by Crowe (Ref. 16):

$$C_d = (C_{dl} - 2) \exp\{-3.07 \gamma^{1/2} (M_R / Re_R) g(Re_R)\} \\ + \{h(M_R) / (\gamma^{1/2} M_R)\} \exp\{-Re_R / (2M_R)\} + 2 \quad (9)$$

where:

$$C_{dl} = \frac{24}{Re_R} (1 + 0.158 Re_R^{2/3}) \quad (10)$$

$$\log_{10} g(Re_R) = 1.25 \{1 + \tanh(0.77 \log_{10} Re_R - 1.92)\} \quad (11)$$

and

$$h(M_R) = \{2.3 + 1.7(T_p / T_f)^{1/2}\} - 2.3 \tanh(1.17 \log_{10} M_R) \quad (12)$$

Individual particle sizes were then numerically tracked through the computational solution. Although the specific size distribution of the atomized alcohol seed used for the test was unknown, results using representative diameters (shown in Fig. 14) agreed qualitatively well in predicting the size and shape of the unseeded core.

$M = 1.95$

$Re_L = 4.48 \times 10^6$

$\alpha = 20^\circ$

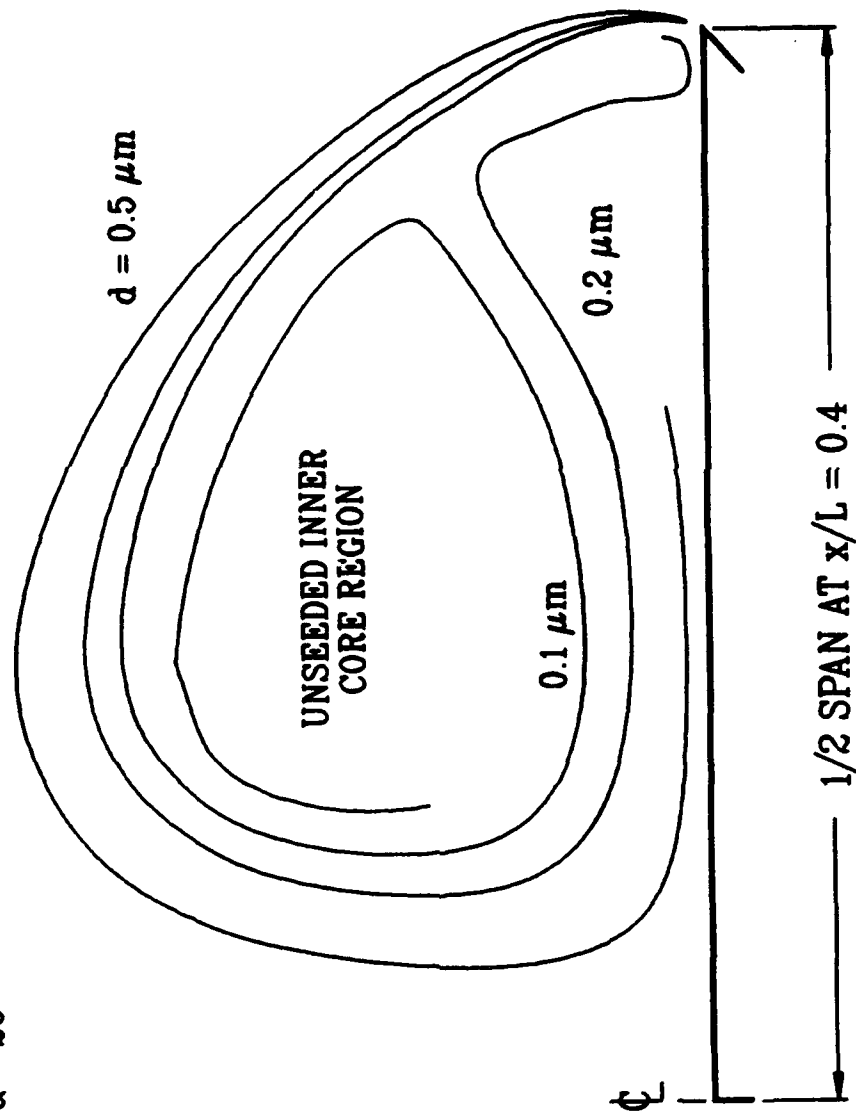


Fig. 14. Particle Trajectories in Mach 1.9 Vortex Flow.

3.3.4 EXPANSION FLOWS AT MACH 6

From these initial tests, the physical ability to acquire supersonic LV measurements became well established, leaving the issue of particle velocity lag as the foremost obstacle in applying LV to complex flows for quantitative results. In addition to the lag evidenced in the cross correlation statistics, through the separation shock at Mach 6, and within the supersonic vortices, high speed expansion turns were also found to be a flow structure affected by this bias (Ref. 17). Shown in Fig. 15 are schematics of two simple model geometries, an axisymmetric ogive-cylinder and a flat plate at 2 degrees angle-of-attack, with representative laser light sheet visualization showing the unseeded regions. Both models were tested in the Mach 6 facility using silicon oil as the seed material. For the ogive-cylinder model, tested at a freestream Reynolds number of 5.3 million per meter, the unseeded portion of the flow starts near the upstream edge of the cylinder and grows to a thickness of approximately 0.5 cm before leveling off near the trailing edge. The flat plate, at a freestream Reynolds number of 10.8 million per meter, shows the unseeded portion of the flow starting at the leading edge, and gradually turning to run parallel to the model surface. In each case, the downstream thickness of the unseeded region is of the same order as the boundary layer thickness, preventing the use of LV to resolve the boundary layer structure.

LV measurements approaching the boundary layers are shown in Fig. 16. For the ogive-cylinder, measurements were collected and processed with the two-dimensional LV system previously applied to Mach 6 flows. The measurements for the flat plate at 2 degrees angle-of-attack were only one-dimensional, but demonstrated that data could be obtained in this regime

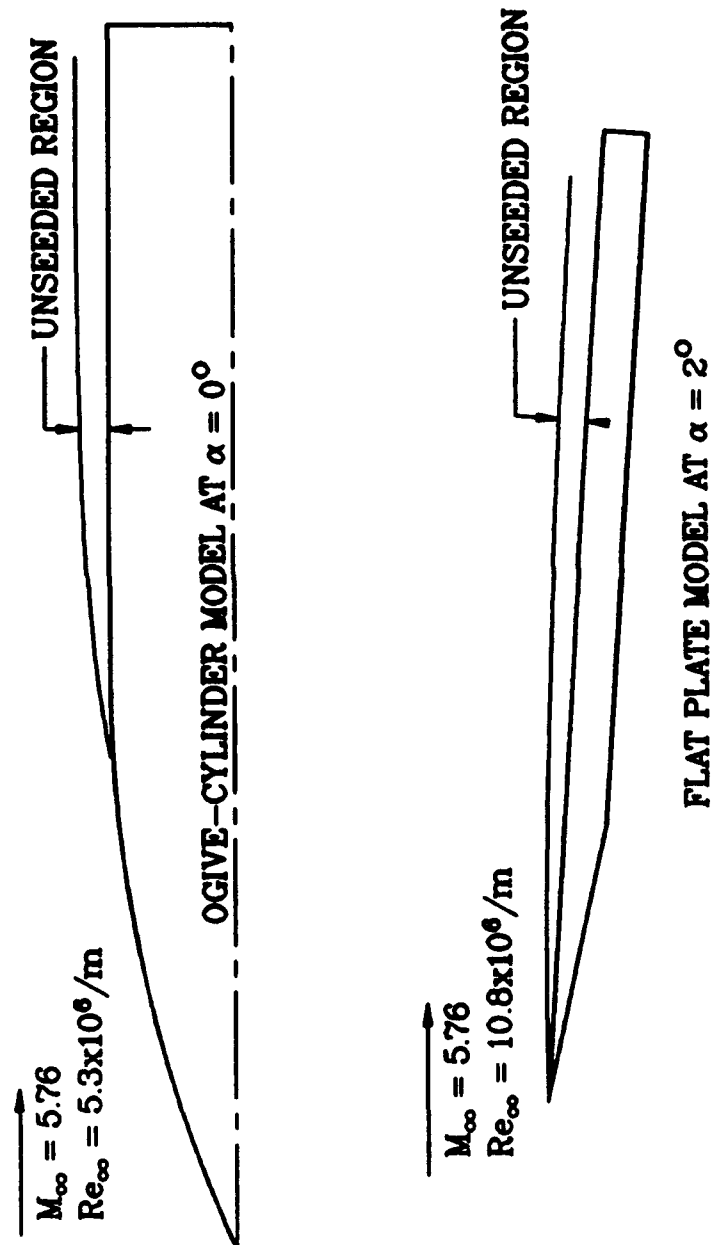


Fig. 15. Unseeded Regions on Ogive Cylinder and Flat Plate at Mach 6.

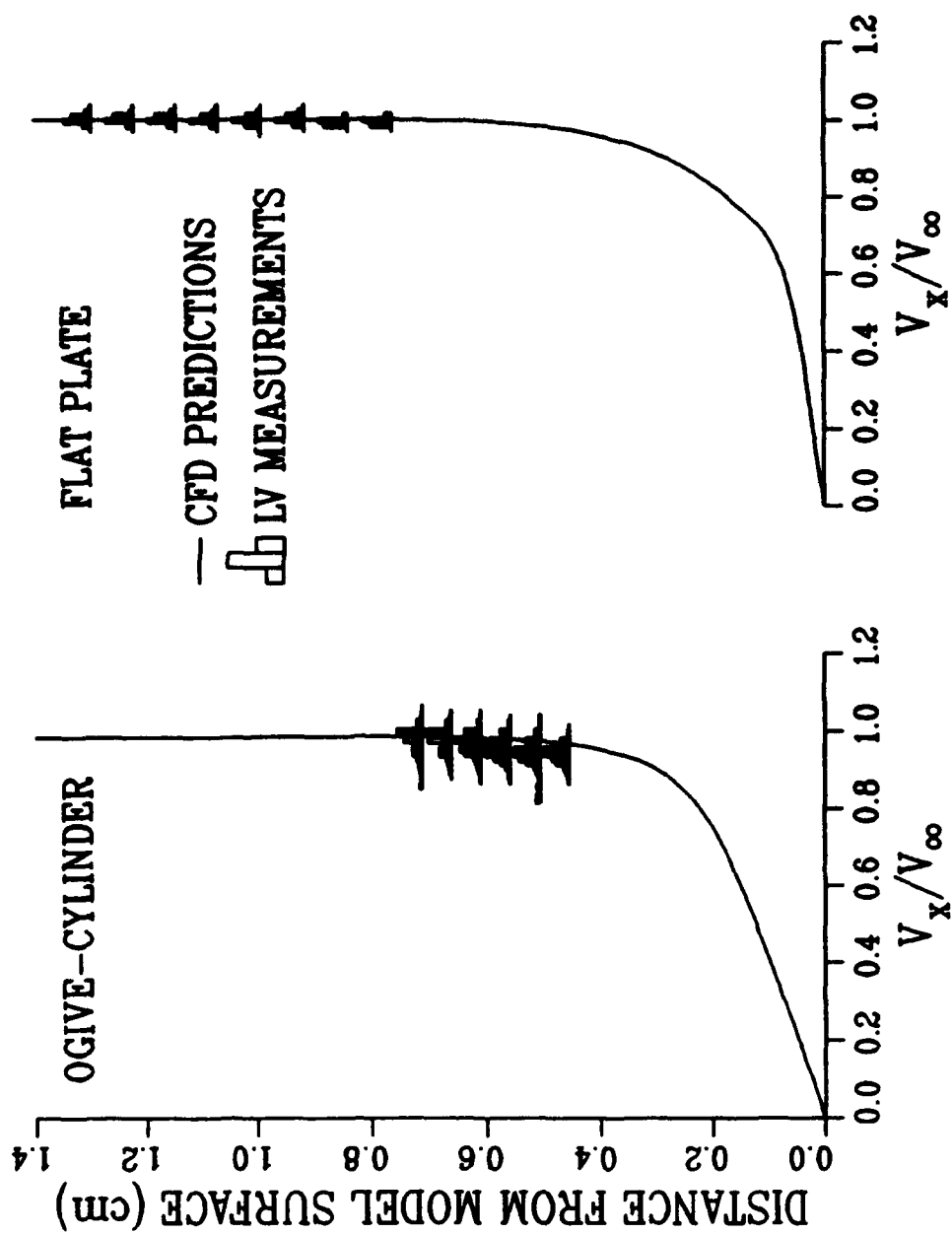


Fig. 16. Velocity Histograms on Ogive Cylinder and Flat Plate at Mach 6.

using a single fiber-optic probe head connected to a Fourier transform type processor. Again, the specific particle size distribution in the flow was not known, but superimposed numerical trajectories of various sized particles through the CFD flowfield solutions were found to qualitatively predict the laser light sheet results.

3.3.5 WEDGE FLOW AT MACH 3

Although analyses of the supersonic vortex and expansion flows were greatly enhanced by utilizing the CFD flowfield solutions, the unknown particle size distributions within those flowfields prevented a direct comparison between the experimental and computational results. Therefore, a methodology was required to specifically quantify the particle size distribution and velocity lag bias so that it could be extracted from the experimental measurements. This was done by using the lag through a shock to estimate the particle size, and then numerically tracking those particles through LV measurement locations throughout the flow (Ref. 10).

LV measurement surveys through the shock wave and boundary layer of a 10 degree half-angle wedge were conducted in the Mach 3 facility using a system similar to that used for previous rough and smooth wall measurements. Surveys through the oblique, two-dimensional leading edge shock, using pure alcohol as seed, exhibited lag in the mean velocity change, but the turbulence intensities were only slightly above freestream values. Consequently, the atomized alcohol seed is nearly monodispersed. Using the measured velocities in conjunction with the particle equation of motion and the ideal, inviscid flowfield behind the shock, the seed diameter is estimated to be 3.6 microns, as shown in Fig. 17.

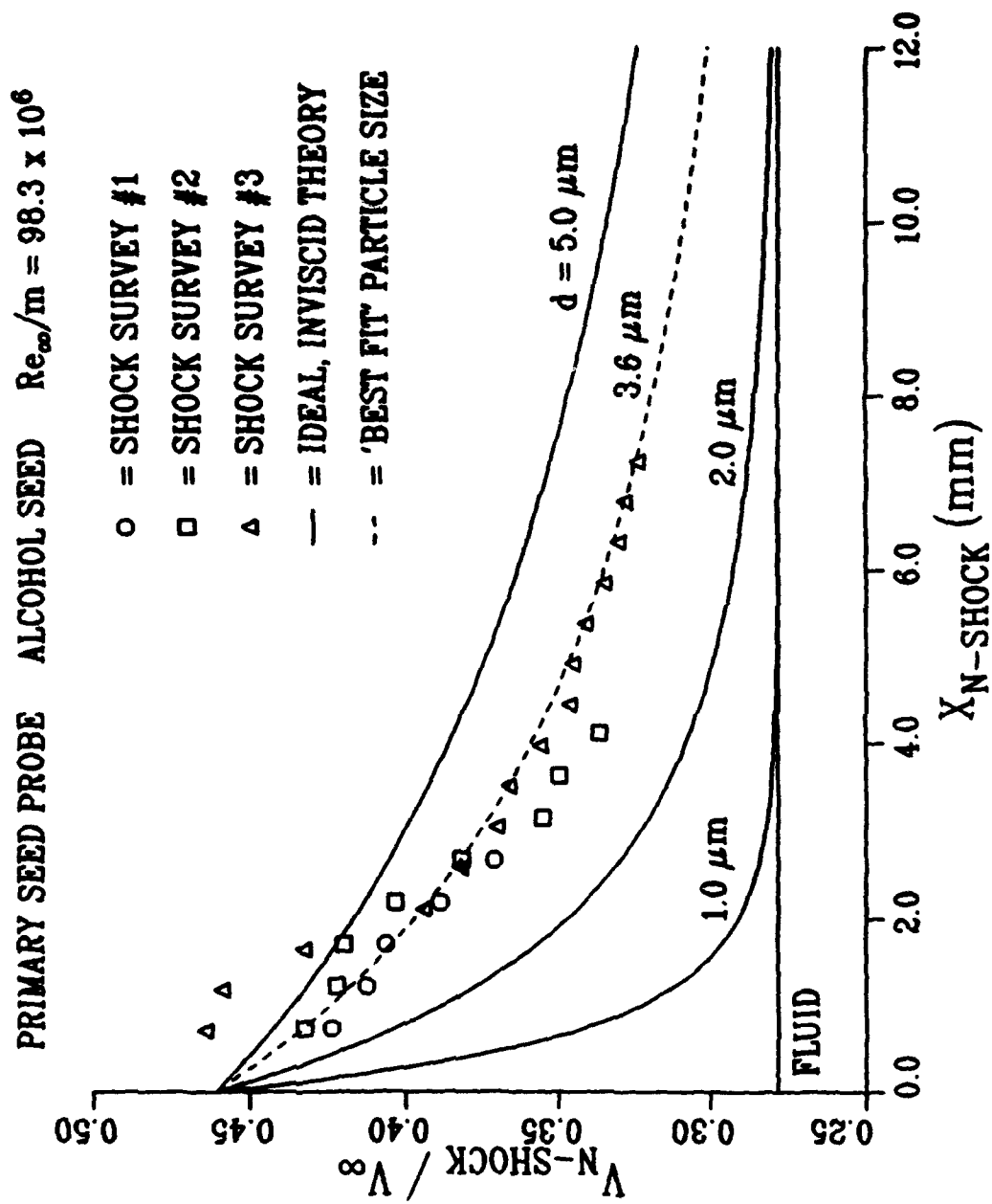


Fig. 17. Particle Size Calculation Through Oblique Shock Wave at Mach 3.

With this estimate of particle size, boundary layer measurements along the wedge were then corrected for velocity lag bias. One such profile is shown in Fig. 18. Outside of the boundary layer, the fluid moves parallel with the wedge, while the seed particles still have a component of momentum towards the surface due to the lag through the leading edge shock. Consequently, the particle velocities are significantly greater than the fluid, and the raw LV measurements compare poorly with the CFD prediction. However, a much more favorable comparison is made after the velocity lag is removed from the data. By applying this analysis, the LV data had quantitative value which otherwise would have been lost.

3.6 INLET FLOW AT MACH 6

The final test to be presented, representing the current state-of-the-art in the application and analysis of LV in supersonic flows is for an inlet configuration at Mach 6 (Ref. 18). This test surpassed the analysis of the Mach 3 wedge test in both the complexity of the flowfield and the ability to account for the polydispersed sizes of the particle diameters.

A schematic of the inlet model along with LV velocity vectors is shown in Fig. 19. The model was tested at a Reynolds number of 44.3 million per meter for cowl inlet angles ranging from zero to 3 degrees. LV measurements were collected at seven profile locations using the two-dimensional system and silicon oil seed material applied to previous tests.

Rather than using the velocity lag through the leading edge shock to determine a mean particle size, as was done with the Mach 3 wedge, these measurements were used to determine the full distribution of particle size concentrations within the flow (Ref. 19). The concept of this

BOUNDARY LAYER SURVEY LOCATION #2

PRIMARY SEED PROBE 3.6 μ m ALCOHOL SEED $Re_{\infty}/m = 98.3 \times 10^6$

□ = MEASURED LV DATA
 ■ = 'CORRECTED' LV DATA
 — = FLUID, BY CFD SOLUTION

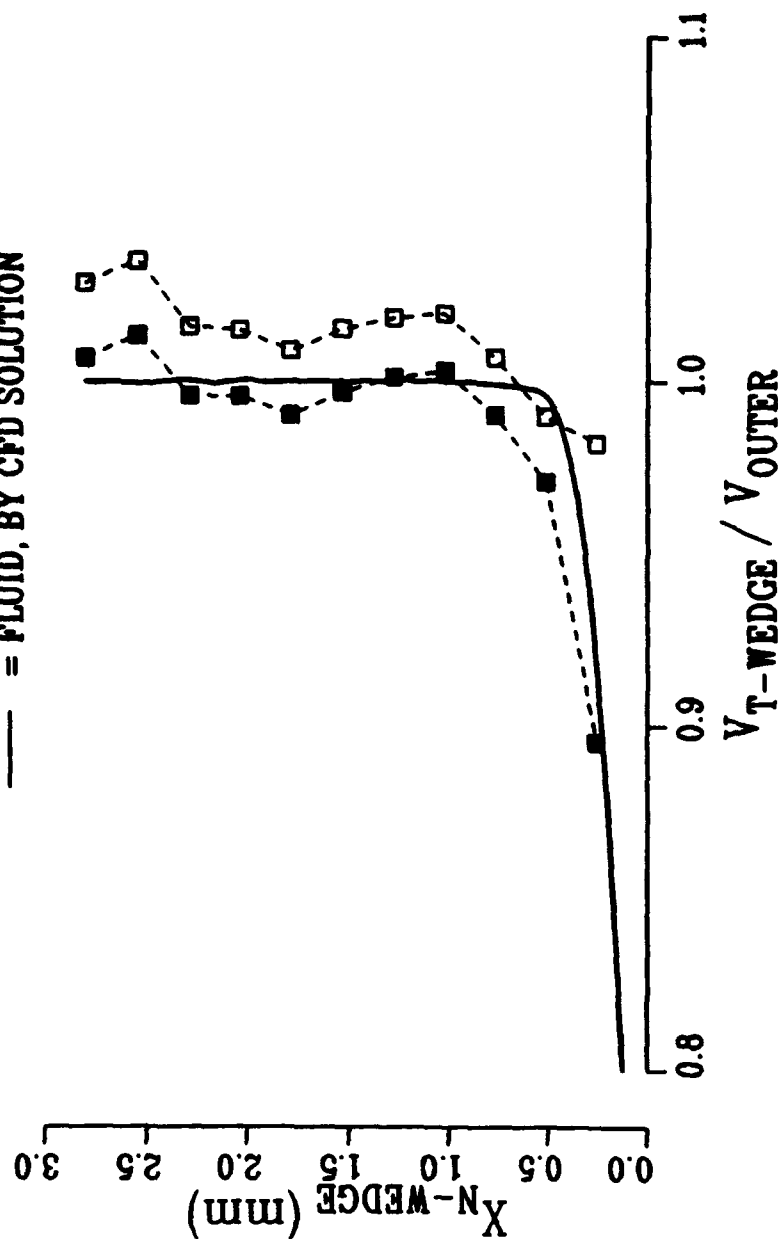


Fig. 18. Boundary Layer Measured and "Corrected" Velocity Profiles on Wedge at Mach 3.

technique is shown in Fig. 20. Since the various particle sizes relax at different rates, the shape of the LV histogram is smeared. However, it can be analytically predicted as a summation of individual Gaussian shapes of different particle diameters, each weighted by their individual concentrations within the flow. Results for this case are shown in Fig. 21 for two resolutions of seed sizes. In each case, particles are found to be primarily in the range of 0.5 to 3.0 microns with a small concentration of particles as large as seven microns.

Knowing the size distribution allowed for the velocity lag bias to be quantified throughout the flow. Results from two of the stations are shown in Figs. 22 and 23. At the cowl entrance, Fig. 22, the LV data validate the computational prediction and is shown to be free of velocity lag bias, except very near the cowl nose. However, the profiles at the throat, Fig. 23, even after accounting for velocity lag, show the CFD solution to have over-estimated the boundary layer turbulence, leading to a predicted profile which is fuller than exists. Thus the CFD solution would over predict the mixing and over predict engine performance.

3.3.7 LV MEASUREMENTS AT MACH 12

To evaluate the potential application of LV techniques to very high speed flows, one-dimensional LV measurements were made in the HWT. The HWT has a contoured nozzle 3.05 m in length and 0.508 m in diameter at the exit where the flow enters the test cabin as a free jet with a freestream velocity of approximately 1466 m/s. In order to assess the applicability of LV in this facility, data were collected in the undisturbed freestream, through the nozzle boundary layer at the exit plane, and through the normal shock region of a bow shock generated by a cylinder. Several types of seed materials, including alumina and a proprietary material,

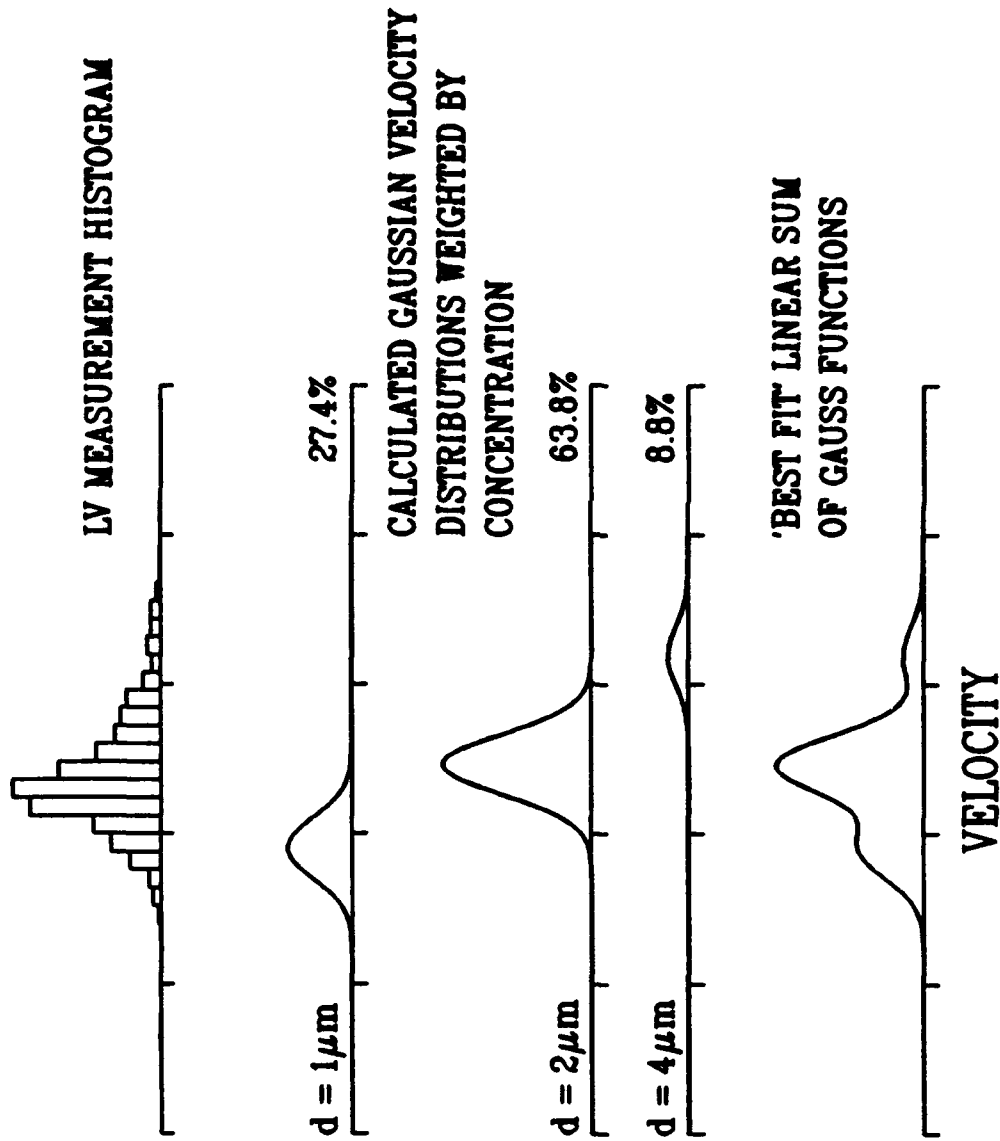


Fig. 20. Concept of Particle Size Distribution Calculations.

SILICON OIL SEED $M_\infty = 5.76$ $Re_\infty/m = 44.3 \times 10^6$

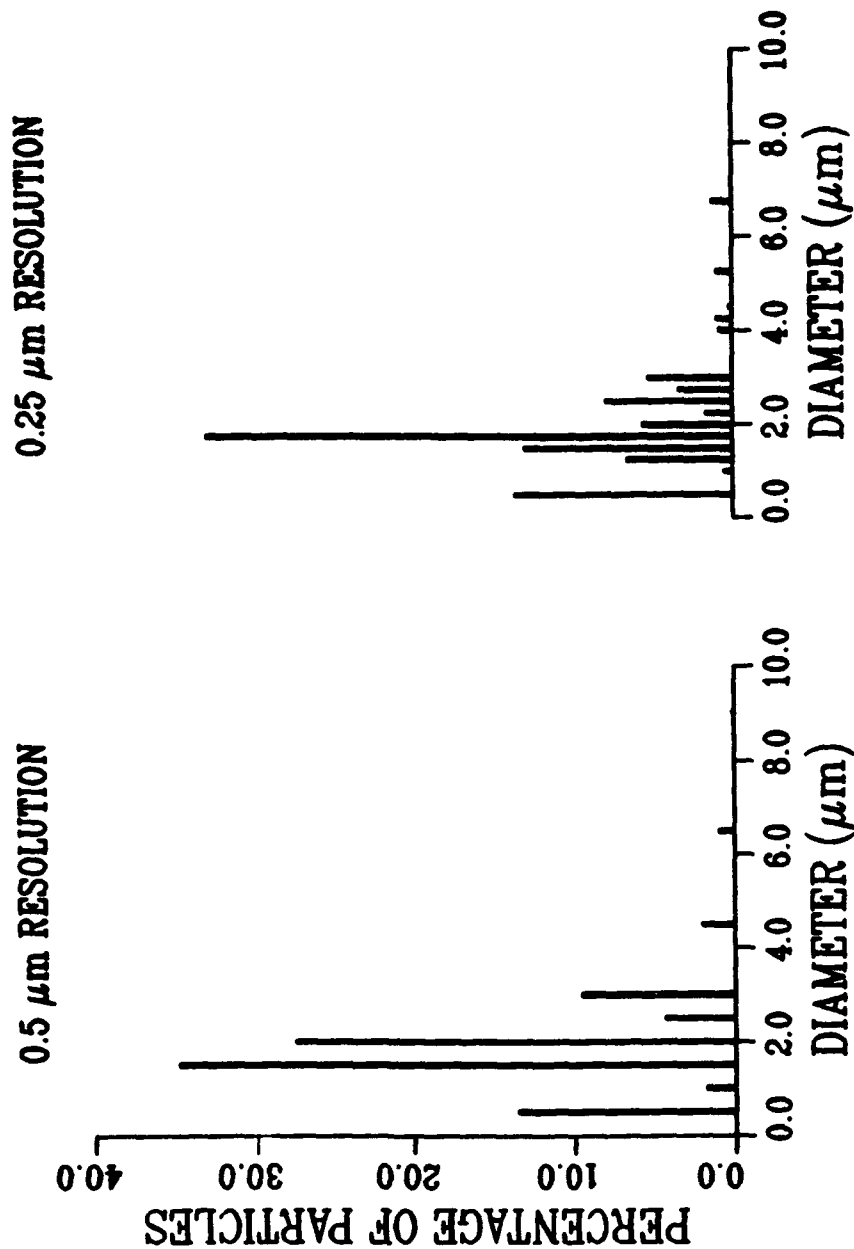


Fig. 21. Particle Size Distribution in Inlet at Mach 6.

— = CFD PREDICTION $M_\infty = 5.76$ $Re_\infty/m = 44.3 \times 10^6$

• = RAW LV DATA $x = 20.27$ cm FOREBODY
 * = 'CORRECTED' DATA - COARSE MESH, COARSE SEED
 + = 'CORRECTED' DATA - COARSE MESH, FINE SEED
 x = 'CORRECTED' DATA - FINE MESH, COARSE SEED
 • = 'CORRECTED' DATA - FINE MESH, FINE SEED

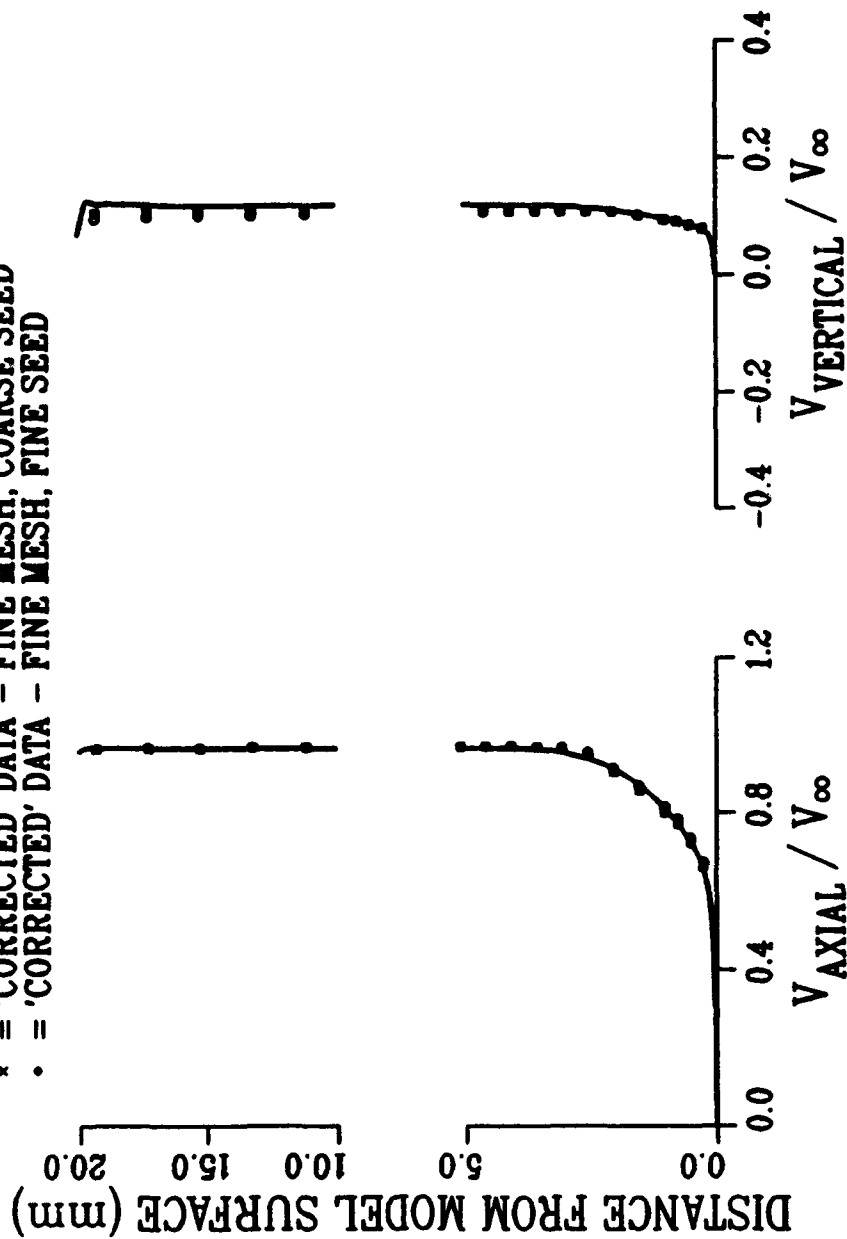


Fig. 22. Measured, Corrected, and CFD Velocity Profiles in Inlet at $x = 20.27$ cm.

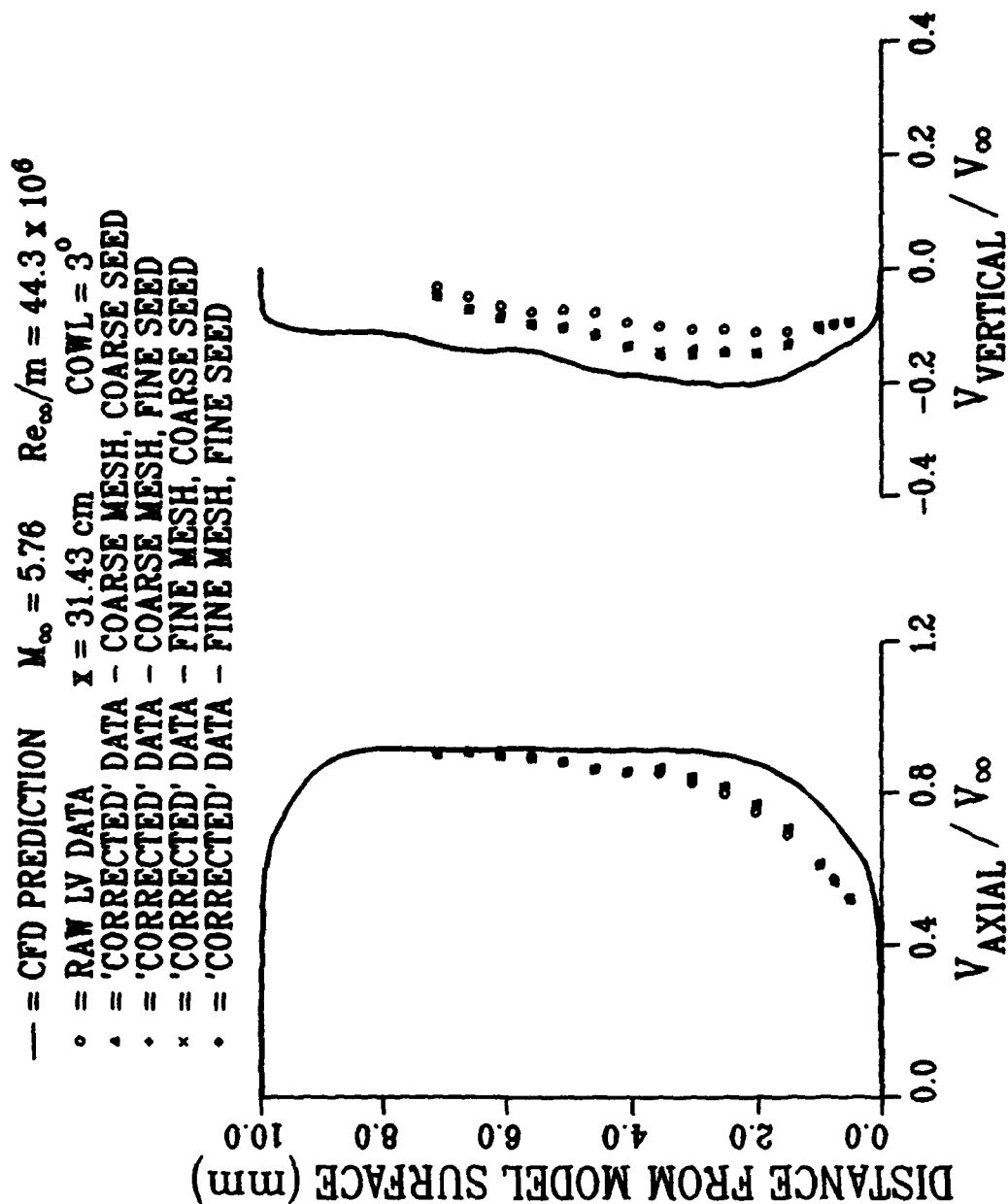


Fig. 23. Measured, Corrected, and CFD Velocity Profiles in Inlet at $x = 31.43 \text{ cm}$.

were examined with emphasis on characterizing the response of particles to gradients in the flowfield and the effect of seeding on the freestream flow.

Mean and rms velocity profiles through the nozzle shear layer are shown in Fig. 24. Data are shown for nominally 1.0 and 0.3 micron alumina and the proprietary seed material. Although all the materials appear to approach the same freestream velocity, there is a significant difference in the particle velocities within the boundary layer. This is due to the different response characteristics of the various seed materials. Computed trajectories for 1.0 micron alumina particles in the nozzle are shown in Fig. 25. It is apparent that particles in the freestream respond slowly to flowfield gradients and are carried into the boundary layer by their own momentum. This results in a measured particle velocity which is greater than that of the local gas velocity. A full analysis of the LV data, including comparison with the computed nozzle and cylinder flowfield and particle trajectories, has been published by Schmisser, et al (Ref. 20). Ref. 20 also includes a description of the fluidized bed seeding system.

3.4 REMAINING LIMITATIONS AND OUTLOOK

The preceding test results demonstrate that the ability to acquire and analyze LV data in the supersonic regime has advanced considerably in the past 5 years, to the point where mean velocity data for complex flows can be used for quantitative flowfield analysis and CFD validation. However, there is ample opportunity for further significant contributions in flow seeding, analysis of velocity lag within turbulence, and continued advancement of optical, mechanical, and electronic system components.

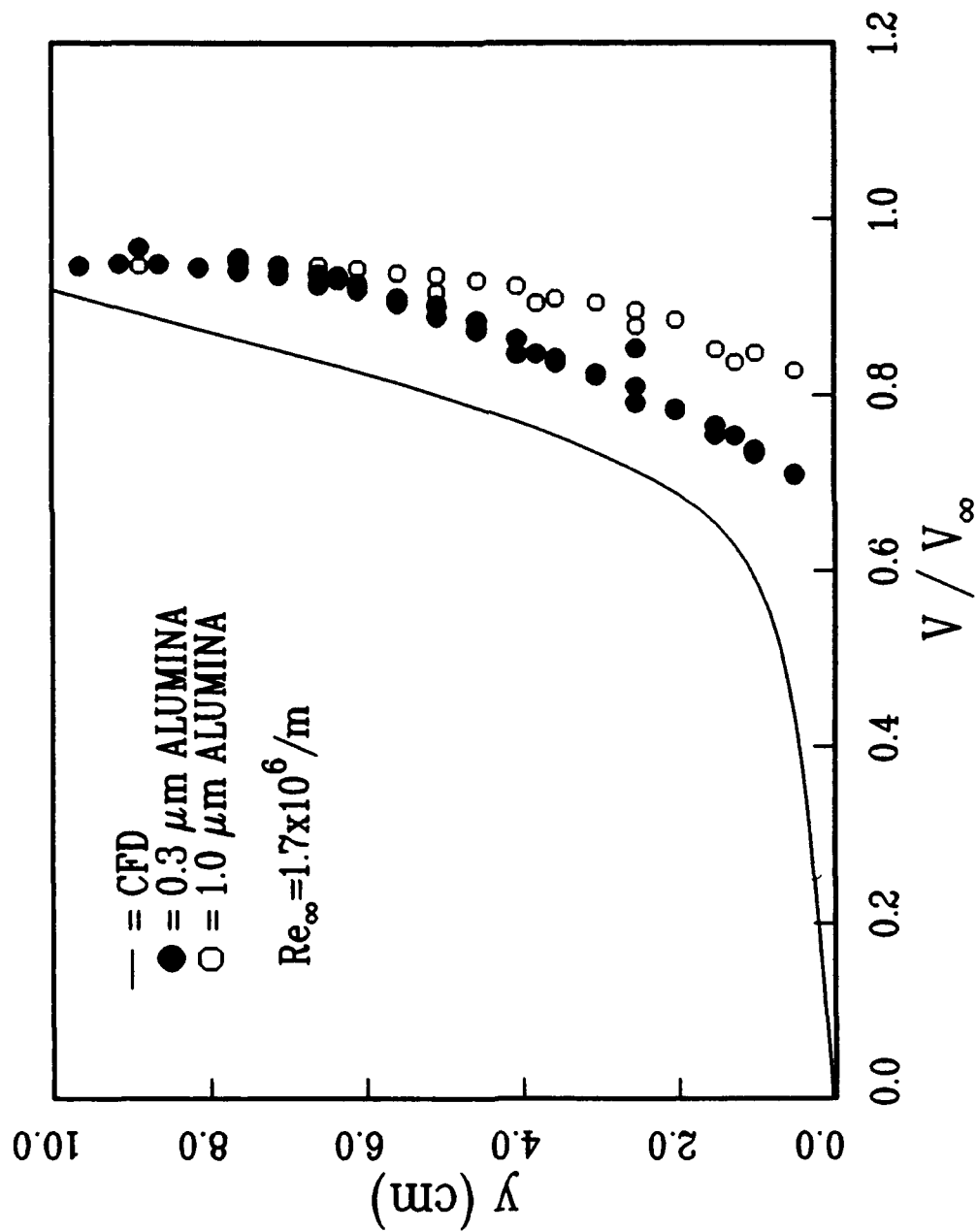


Fig. 24. RMS and Mean Velocities Through Shear Layer at Mach 12.

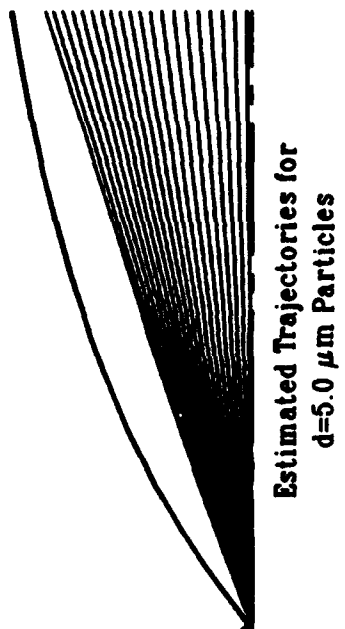
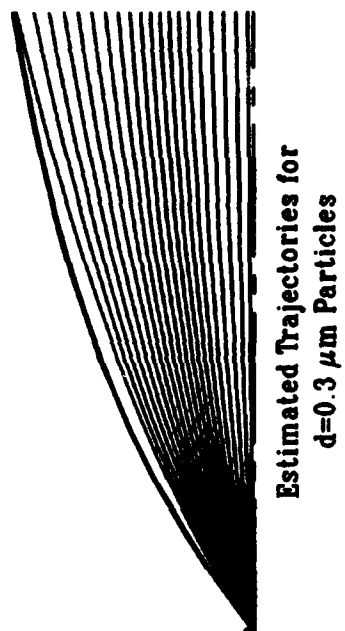
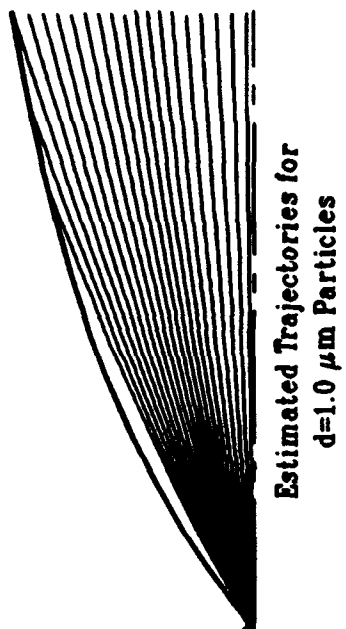
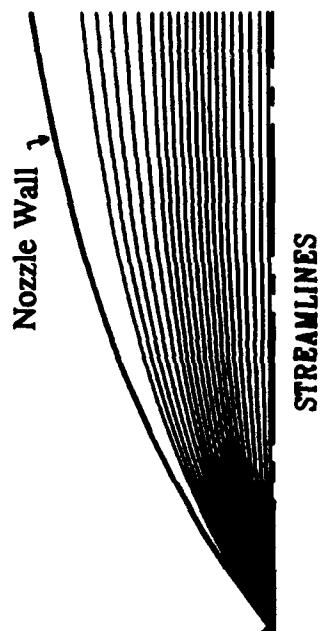


Fig. 25. Computed Trajectories for Alumina Particles through Nozzle Expansion.

Eventually, this type of data may be acquired more easily using one of the molecular based techniques being developed. However, in the mean time, LV will continue to provide critical data and will continue to develop as a state-of-the-art technology in the supersonic regime.

4.0 LASER INDUCED FLUORESCENCE AND RAYLEIGH SCATTERING

In most high speed wind tunnel facilities, the gas used passes through a heater element and is then cooled to low local temperatures in the expansion process. This expansion process can leave some of the gas trapped in an excited vibration state. The resultant nonequilibrium gas may be detected using nonintrusive optical techniques such as laser induced fluorescence (LIF) and Rayleigh scattering. LIF capitalizes on the fluorescent excitation of oxygen molecules present in the flow medium to obtain measurements of temperature and density.

In LIF, fluorescent excitation is accomplished using two laser pulses at frequencies resonant with distinct transition components. A schematic of the laser system is shown in Fig. 26. A standard Nd:YAG laser producing a frequency doubled 532 nm beam is used to pump two oscillator-amplifier dye lasers. The two output beams from the dye lasers are temporally separated by means of unequal optical path lengths.

Each beam is frequency doubled through a BBO crystal then frequency tripled by mixing crystals to produce the desired frequency of 206 nm. The two beams are combined using a polarization optic. The combined beam passes through a gas reference cell containing air at a pressure and temperature comparable to that of the nonequilibrium gas located in the test section. The reference cell provides the signal needed to normalize the actual sample signals from small variations in the relative laser pulse energies. The laser beam exiting the reference cell is directed into the wind tunnel, through a 7 cm diameter fused silica window. After the laser

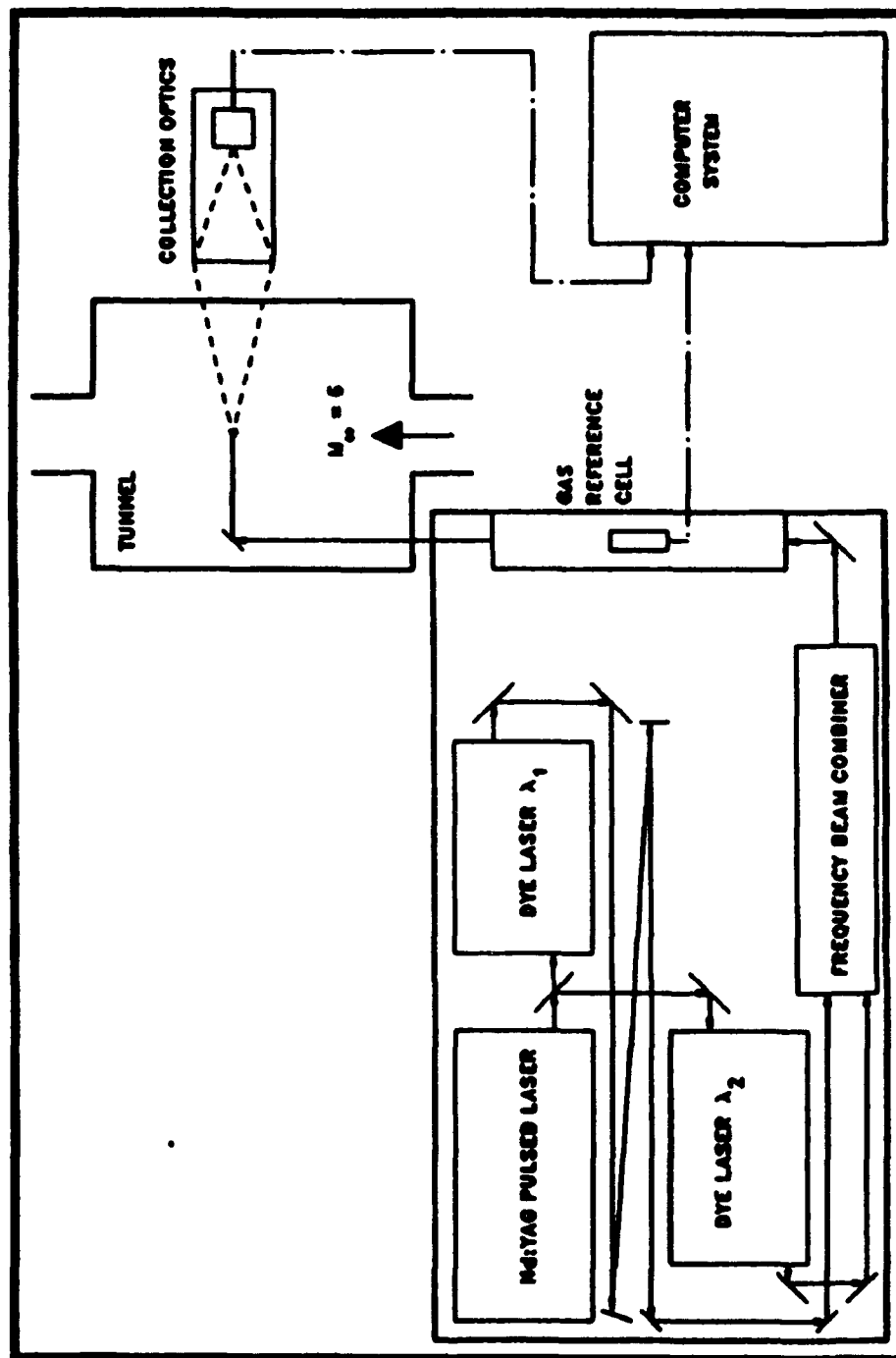


Fig. 26. Laser Induced Fluorescence System Schematic.

beam enters the tunnel, it is steered using two 90-degree turning prisms, mounted on a three-dimensional traverse system, such that the beam impinges on the test model.

Since the two excitation pulses are separated slightly in time, the resulting signals from each individual excitation occur with a slight time offset and can be recorded efficiently by a single photomultiplier tube (PMT) mounted on each of the reference cell and wind tunnel collection systems. The collection system for the reference cell remains fixed. The collection system for the wind tunnel signal is mounted on a three-dimensional traverse capable of tracking with the tunnel traverse steering the laser beam. This tracking system allows three dimensional measurements in the Mach 6 HRNF. The output of each collection system is amplified and read by two gated integrators. The temporally separated fluorescence signals are selectively gated by offsetting the gate for the integrators to match the offset of the two excitation laser pulses. The microcomputer reads the integrated signals and processes them.

The ratio of the intensity of the two signals from the reference cell define a normalization factor against variations in laser pulse energies. This normalization factor is applied to the intensity ratio of the two signals from the sample measurement. This corrected intensity ratio can be transformed into a temperature measurement for the sample point. Since the density will reflect the random error noise that appears in the temperature measurement, the intensity of the signals must be corrected for temperature. Then the absolute intensity of the signals can be used to determine the sample density since the number of excited oxygen molecules scales directly with density (Ref. 21).

The initial tests of the LIF technique were difficult to perform because of excessive scattered light and fluorescence off the tunnel walls and the model surface. The scattered light was apertured down in the collection optics resulting in a reduced signal level which was difficult to read. In an attempt to obtain some measurements in the Mach 6 HRNF, the Rayleigh scatter system, being a less complicated system, was configured. The Rayleigh scatter system is less complicated for several reasons. Rayleigh scattering deals with light scattered off a molecule versus fluoresced excitation of a molecule, thus the system is not dependent on laser frequency. This independence permits the use of one laser beam instead of two resulting in an easier alignment procedure. Also, temperature measurements are not attempted with Rayleigh scattering, only density measurements are made, thereby easing the resulting computations. The temperature measurement obtained from LIF techniques will be attempted after further development of the system has been accomplished. The development stage of these systems will be performed using Rayleigh scattering since the implementation of the Rayleigh scatter system is simpler than that of the LIF system.

In an effort to determine what effect a pulsed laser beam impinging on a stainless steel model surface has on the collected scatter signal, a test model, initially removed from the measurement region, was repeatedly placed in and removed from the measurement region. The measurements were made in atmospheric conditions for a no flow situation. The results of this experiment are shown in Fig. 27. The injection of the test model into the measurement region results in a 20 percent increase in the signal level, approximately. Future tests will involve the use of filters to block the scattered light off the test model thus decreasing, possibly eliminating, the signal level increase associated with injecting the model into the measurement region. So

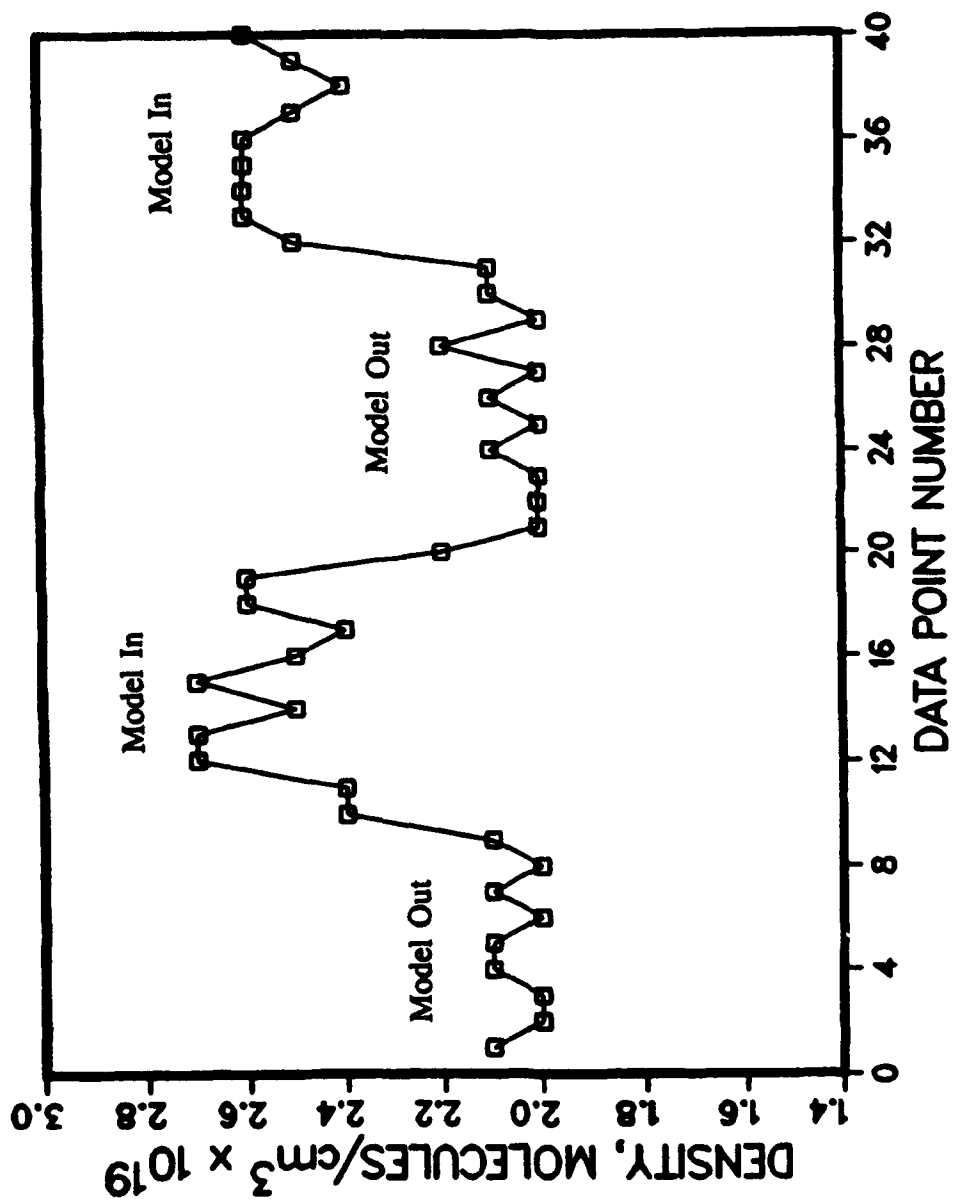


Fig. 27. Density Distribution Measured as Model is Injected and Removed Repeatedly.

far, unaffected measurements have been obtained at approximately 1.25 cm off the model surface without the use of filters.

Questions concerning the measurement capability for the lower limit of density values inspired the next experiment. For this experiment, the model was removed from the test chamber to avoid any detrimental effects associated with beam impingement on the model. The test chamber was then slowly pumped down to a vacuum condition. Rayleigh scatter measurements were performed during the pump-down process, tracking the pressure of the air in the test chamber to its lower limit of 344 Pa, according to readings from static pressure probes in the tunnel. These tracking measurements are shown in Fig. 28. A density value of $2.5\text{E}+19$ molecules/cc corresponds to standard atmospheric pressure and temperature conditions. After remaining at a vacuum for some time, the test chamber was vented back to atmosphere. However, a stuck valve prevented the chamber from venting completely. This difficulty in venting is apparent in Fig. 29 as the slight increase in density measurement around data point number 70. Again the test chamber was pumped down to a near vacuum and then vented completely. The Rayleigh scatter density measurements initially overshoot the atmospheric value only to settle down to the expected reading, as shown in Fig. 29. One possible cause of this overshoot in the reading is dust particles transported into the test chamber during the venting process.

With the results of the previous experiment concerns about condensation effects (Ref. 22) and possible clustering of oxygen molecules surfaced (Ref. 23). The tunnel was operated at a set stagnation temperature of 508.3 K and various stagnation pressures, 1.724, 1.379, 1.034, 0.689 MPa. The results of this experiment are shown in Fig. 30. Assuming the isentropic

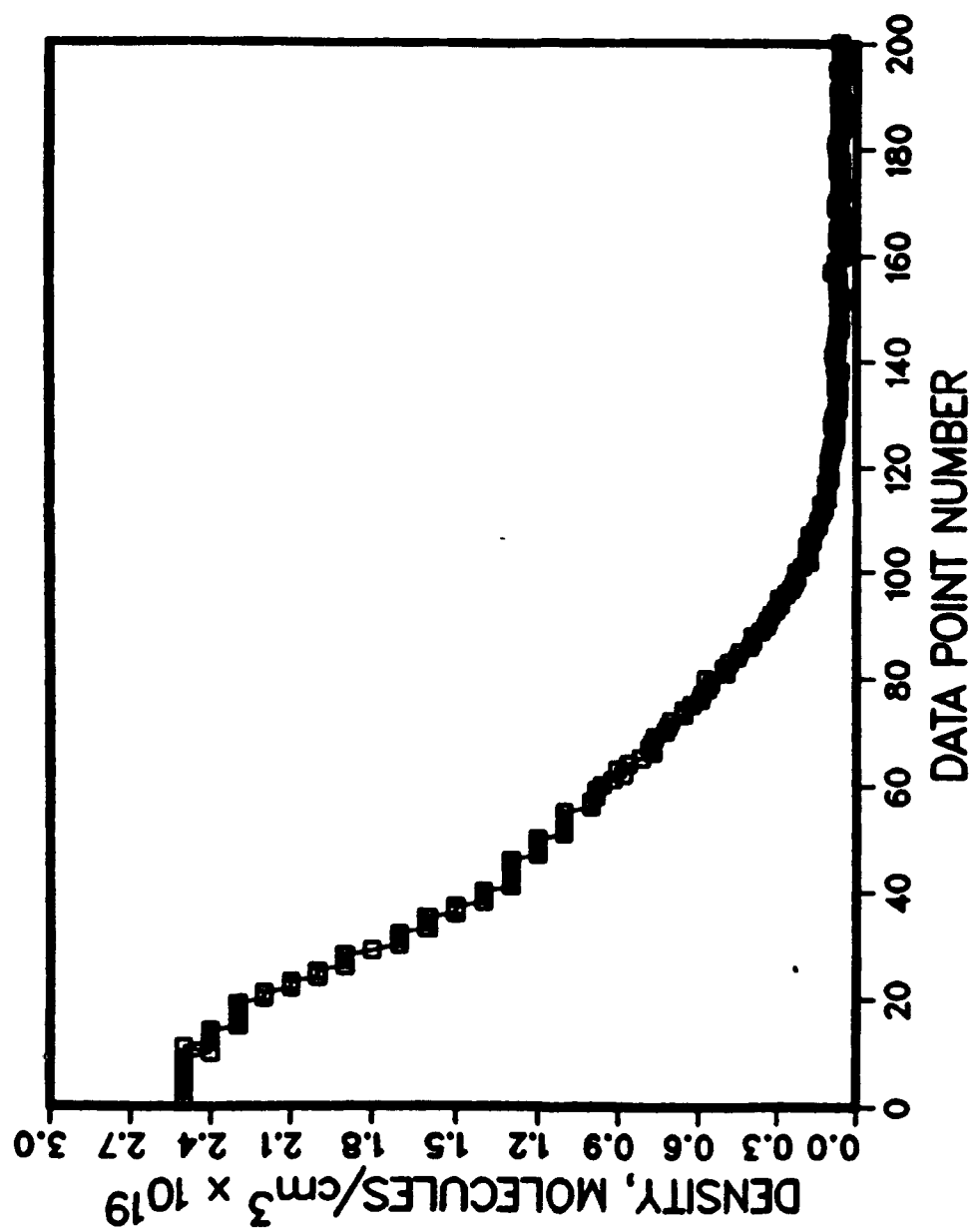


Fig. 28. Density Distribution Measured as the Tunnel is Pumped Down to Vacuum.

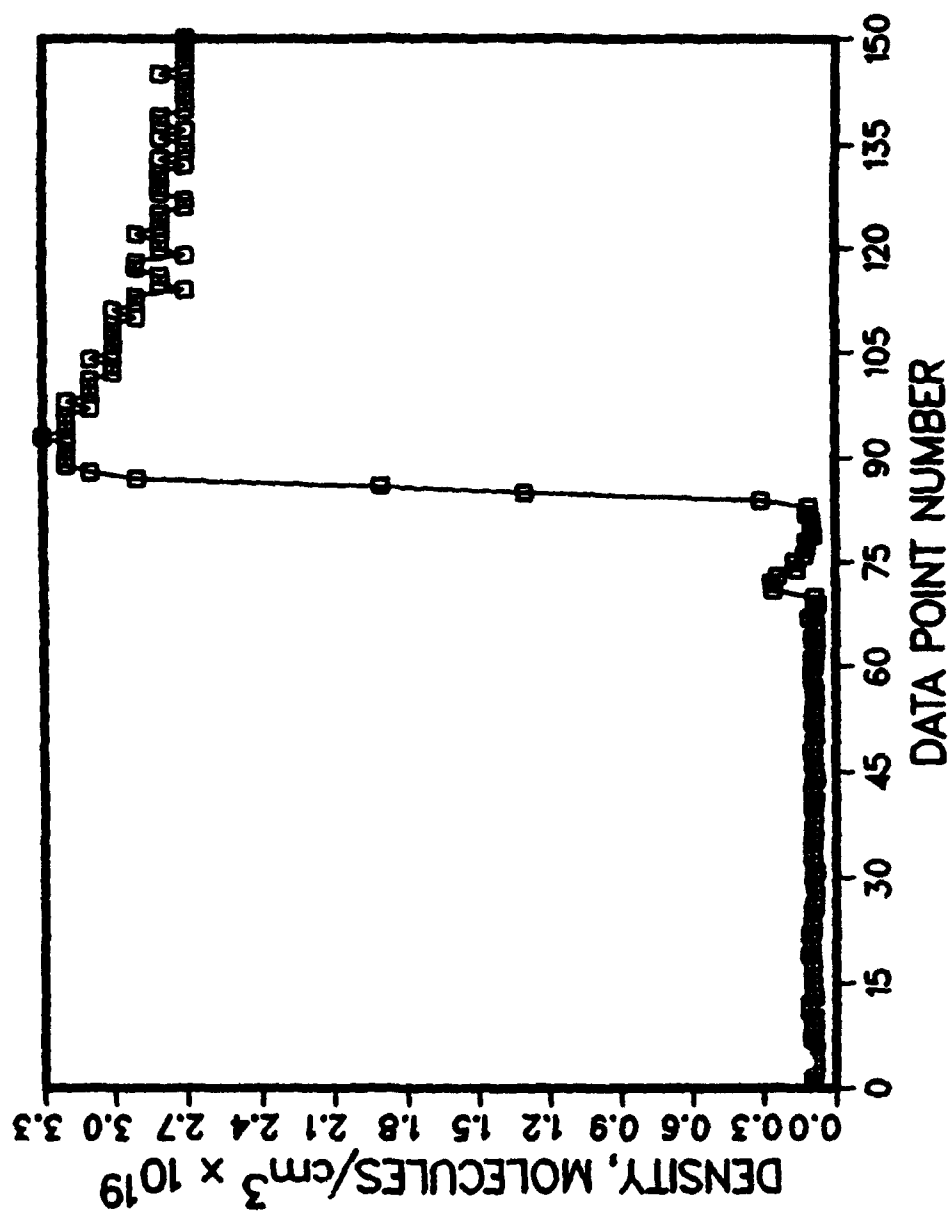


Fig. 29. Density Distribution Measured as the Tunnel is Vented to Atmospheric Pressure.

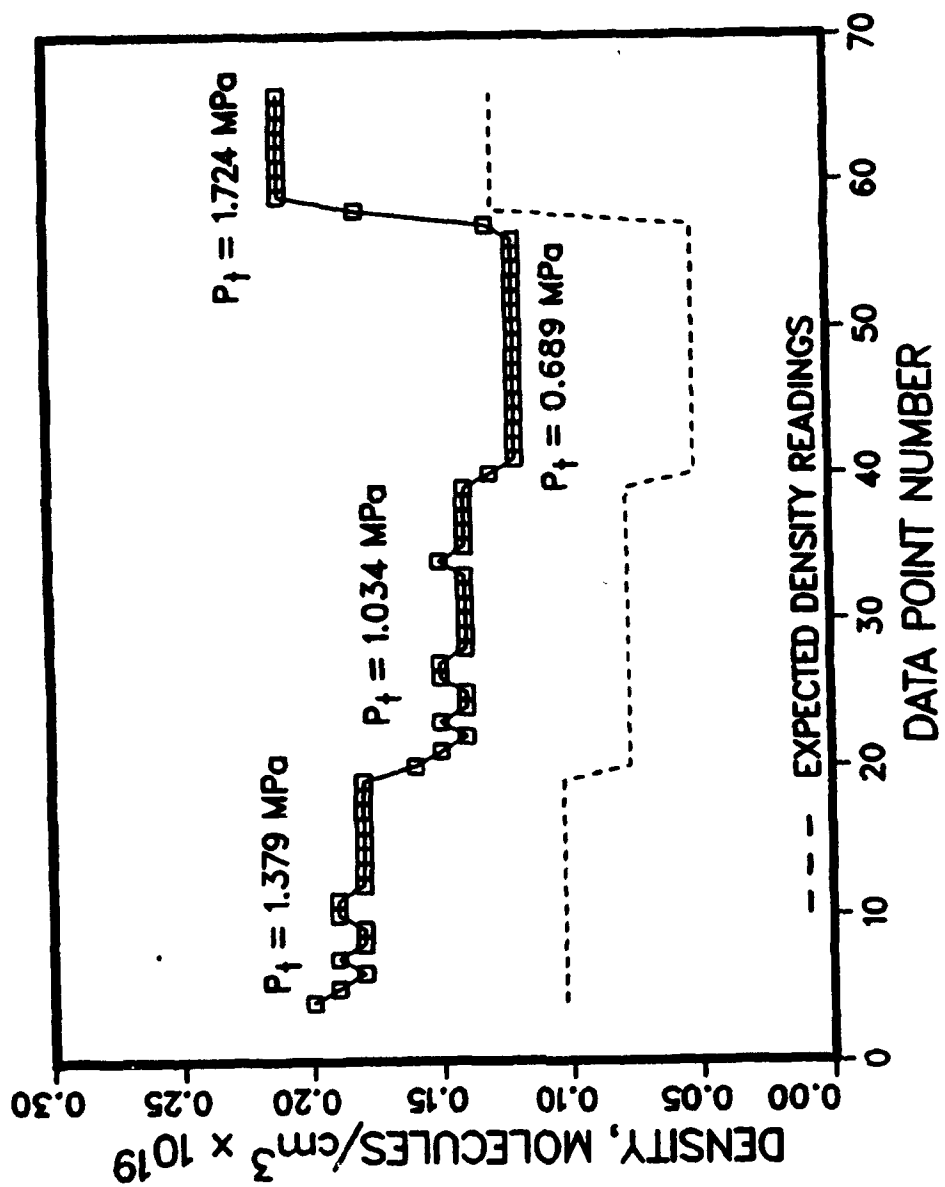


Fig. 30. Density Distribution at Several Pressures.

process is applicable, it may be determined that the measured densities for the various stagnation pressures were higher than expected by approximately 40-50%. This measurement error is unacceptable. It is believed that condensation and stray particles in the freestream were the cause of this error in the measurements. Future tests will attempt to verify this analysis or determine the cause of the error.

5.0 PHASE SHIFT HOLOGRAPHIC INTERFEROMETRY

Holographic interferometry was initially developed for use in the Wright Laboratory in the 1970s. However, due to the difficult and time consuming data reduction process the technique has not been used extensively since the development of the laser velocimetry systems. Significant advances in computer performance and digital scanning cameras have lead to the development of phase shift holographic interferometry and Fourier transform interferometry methods (Ref. 24) for use in wind tunnel experiments.

The phase shift technique is based on the research of Carré (Ref. 25) and Bruning, et al. (Ref. 26), among others. But it was the work of Creath (Ref. 27) that has brought phase shift interferometry to the point where this technique can be applied in fluid dynamics research. The phase shift holographic interferometry technique has been demonstrated in the wind tunnels at the Naval Surface Warfare Center by Spring (Ref. 28) et al for a simple supersonic axisymmetric body and a complicated two-dimensional scramjet inlet.

The fundamental equations (Ref. 27) of phase shift interferometry are a set of simultaneous equations for the intensity

$$I_1(x,y) = I_0(x,y) [1 + \gamma \cos(\phi + \frac{\pi}{4})] \quad (13)$$

$$I_2(x,y) = I_0(x,y) [1 + \gamma \cos(\phi + \frac{3\pi}{4})] \quad (14)$$

$$I_3(x,y) = I_0(x,y) [1 + \gamma \cos(\phi + \frac{5\pi}{4})] \quad (15)$$

which can be solved to yield the phase ϕ , modulation γ , and background intensity I_0 . For this set of equations the phase is calculated as

$$\phi(x,y) = \tan^{-1} \left[\frac{I_3(x,y) - I_2(x,y)}{I_1(x,y) - I_2(x,y)} \right] \quad (16)$$

The quadrant of ϕ is determined by analysis of the signs of the numerator and denominator of the argument in Eq. (16). The difficulty in solving the phase shifted images is the 2π ambiguity inherent in the inverse tangent. To correct for the ambiguity, adjacent pixel values are compared and if a phase jump of π or greater is present, then one of the values is adjusted by adding or subtracting 2π thus yielding a continuous phase distribution map.

Once the phase map of the field has been calculated, the density may be calculated from the phase map. The phase is related to the index of refraction by

$$\phi(x,y,z) = \frac{2\pi}{\lambda} \int_0^L [n(x,y,z) - n_0] dz \quad (17)$$

and the index of refraction (n) is converted to density (ρ) using the Gladstone-Dale relation (Ref. 29) where K is the Gladstone-Dale constant.

$$n - 1 = K\rho \quad (18)$$

For a two-dimensional flowfield the density may be considered constant along a ray of light through the tunnel and the density is calculated from

$$\frac{\rho(x,y)}{\rho_0} = 1 + \frac{\phi(x,y)\lambda}{2\pi\rho_0KL} \quad (19)$$

For axisymmetric flows a more complicated calculation must be performed using the coordinate system shown in Fig. 31. In this coordinate system,

$$z = \sqrt{r^2 - y^2} \quad (20)$$

Using the substitution

$$f(x,r) = K [\rho(x,r) - \rho_0] \quad (21)$$

the phase relationship for axisymmetric flows may be written as

$$\phi(x,r) = \frac{2\pi}{\lambda} \int_y^R \frac{rf(x,r)}{\sqrt{r^2 - y^2}} dy \quad (22)$$

This relationship may be inverted using the Abel inversion technique (Ref. 30) to yield

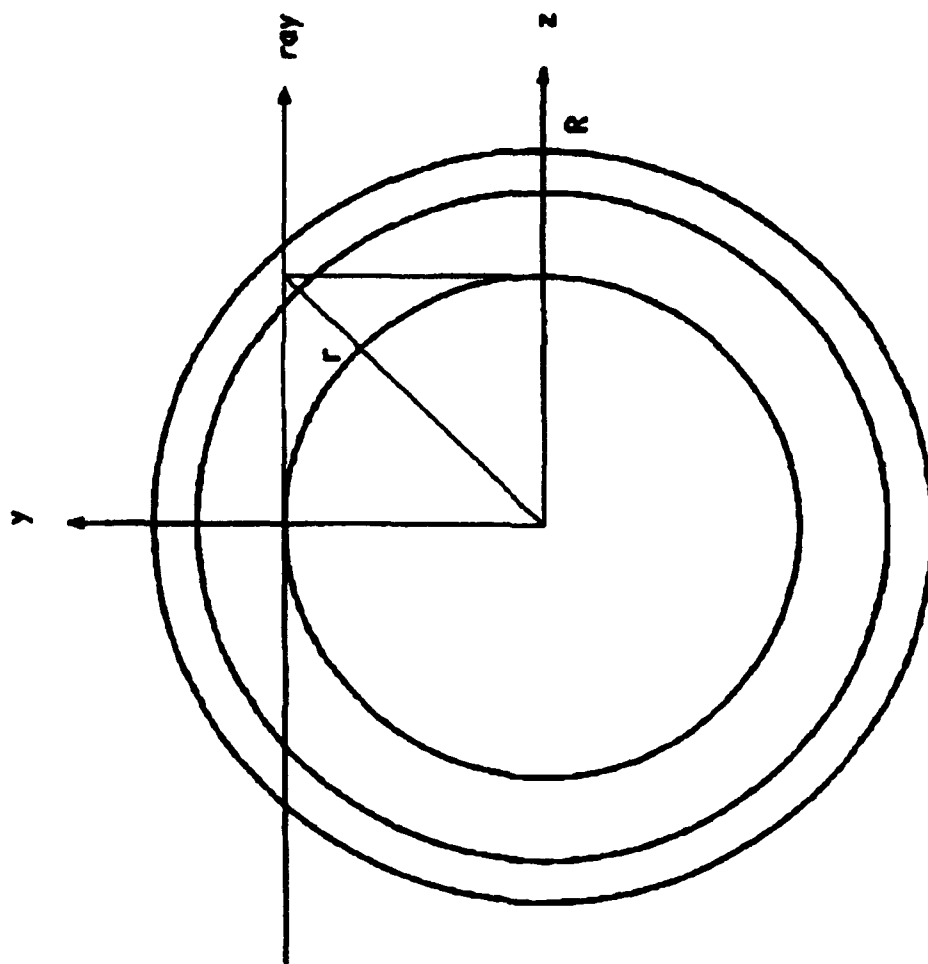


Fig. 31. y, z, r Coordinate System.

$$f(x,r) = -\frac{\lambda}{2\pi^2} \int_r^R \frac{d\phi/dy}{\sqrt{y^2-r^2}} dy \quad (23)$$

such that the density is calculated as

$$\rho(x,r) = \frac{1}{K} f(x,r) + \rho_0 \quad (24)$$

Further details are given by Spring (Ref. 28) et al. for calculating these equations numerically.

The dual reference beam holographic interferometer used at the Wright Laboratory is shown schematically in Fig. 32. In this interferometer, one reference beam is used to shoot a reference wave front of the test article with no flow in the wind tunnel. The second reference beam is then used to shoot the wave front of the test article with flow in the tunnel. The angle between the reference beams is duplicated in the reader system shown in Fig. 33. The two paths of the reference beams are used for the phase shifting process. One of the reference beams is phase shifted using a piezo-electric controlled translation of a mirror thus producing a path length difference and phase shift. The reader system includes a second interferometer which is used to calibrate the phase shifting process and precisely determine the $\pi/4$, $3\pi/4$, and $5\pi/4$ phase shifts.

At each phase shifted state the holographic image is digitized using a CCD camera. It is the intensity values obtained from these digitized images that are used in Eqs. (13), (14) and

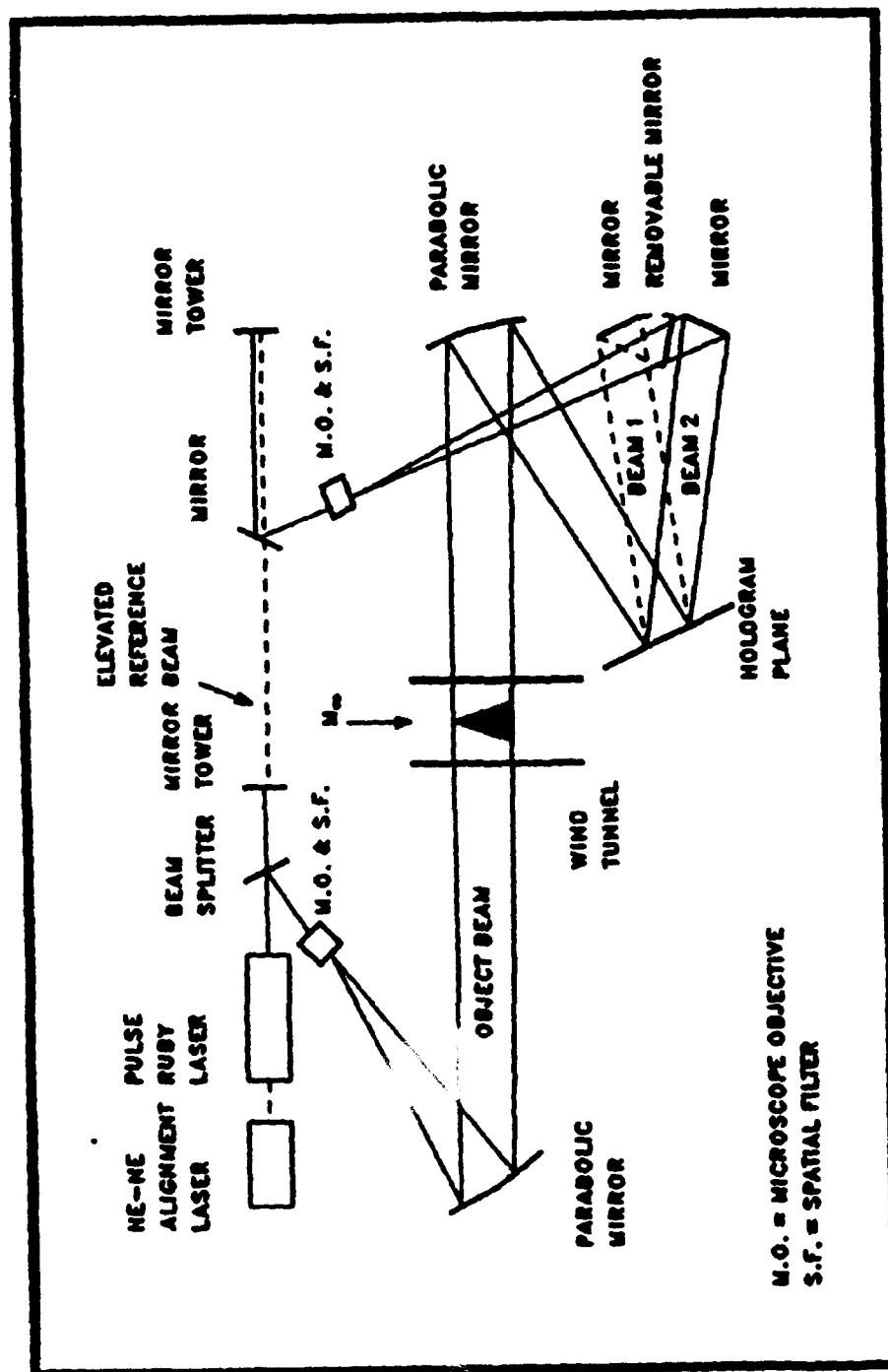


Fig. 32. Phase Shift Holographic Interferometry Writer System.

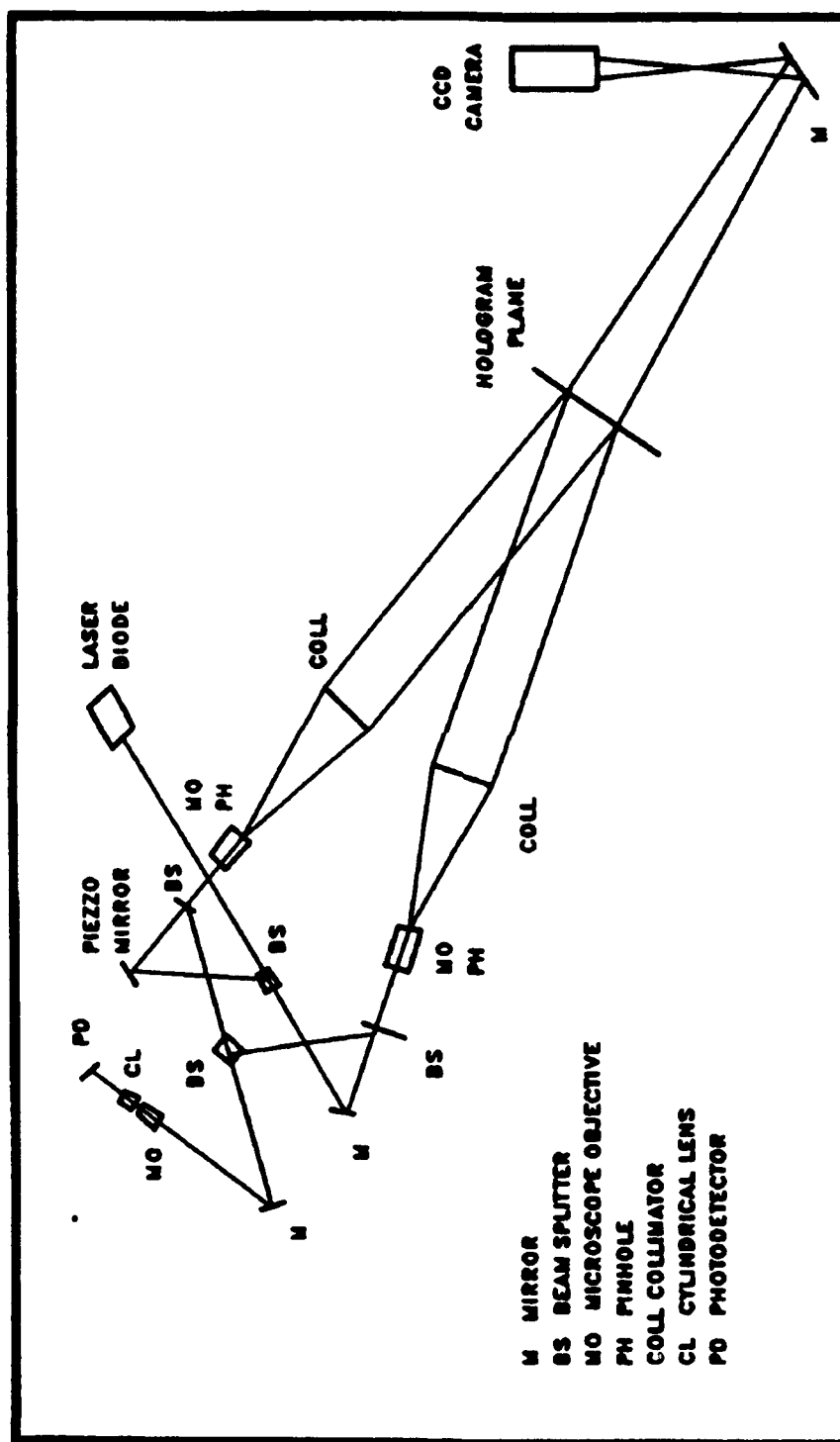


Fig. 33. Phase Shift Holographic Interferometry Reader System.

(15) to obtain the raw phase map. A true phase map is then computed by removing the 2π ambiguities. Eq. (19) or Eqs. (23) and (24) are then applied to compute the density distribution in the flowfield.

Initial experiments have been made in the Mach 3 HRNF with a 10 degree half-angle wedge as the test article. This simple model was used for purposes of system development, data reduction development, and ease of validation. A schematic of the wedge model and its flowfield is shown in Fig. 34. An infinite fringe interferogram of the flowfield is shown in Fig. 35 as captured by a video monitor. A companion finite fringe interferogram and a shadowgram generated by optical manipulation of the reader system are shown in Figs. 36 and 37, respectively. Note the turbulence level evident in the freestream on the Mach 3 HRNF at this stagnation pressure. The data reduction software is being developed.

After full validation of the results from the wedge, experiments will be conducted with models with increasingly complicated flowfields. It is anticipated that difficulties will arise in data reduction algorithms as the flowfields become more complicated than the simple flowfield on the wedge. Attempts to use companion computational fluid dynamics results for trend analysis will be made for more complicated data analysis algorithms.

After development of the phase shift holographic interferometry system in the Mach 3 high Reynolds number facility, the system should easily transition to the Mach 6 HRNF and the Trisonic Gasdynamics Facility. It should be noted that the interferometry technique is limited to use on two-dimensional and axisymmetric flowfields. Tomographic techniques are required for three-dimensional flowfields.

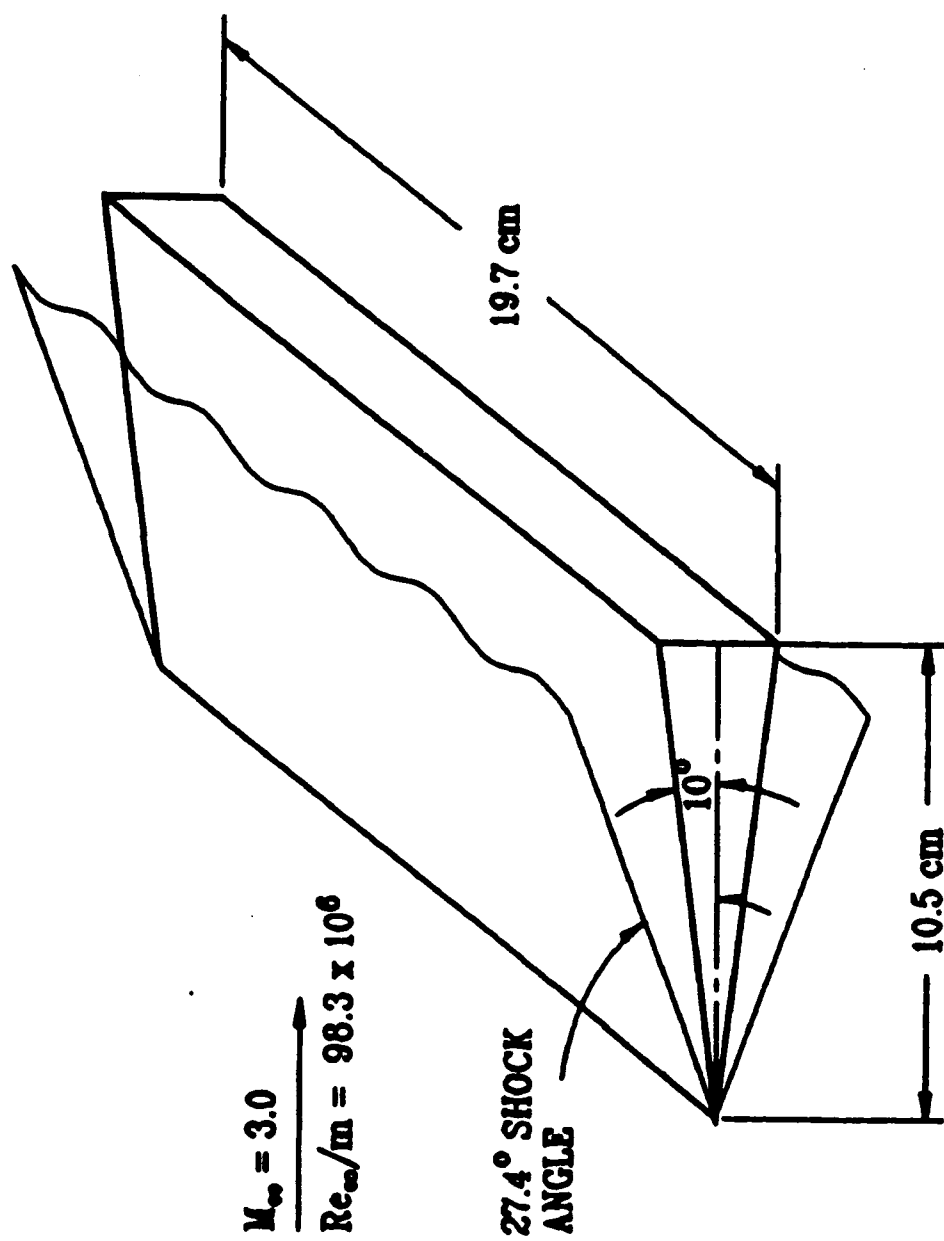


Fig. 34. Schematic of Wedge and Flowfield.



Fig. 35. Infinite Fringe Interferogram of Wedge at Mach 3.

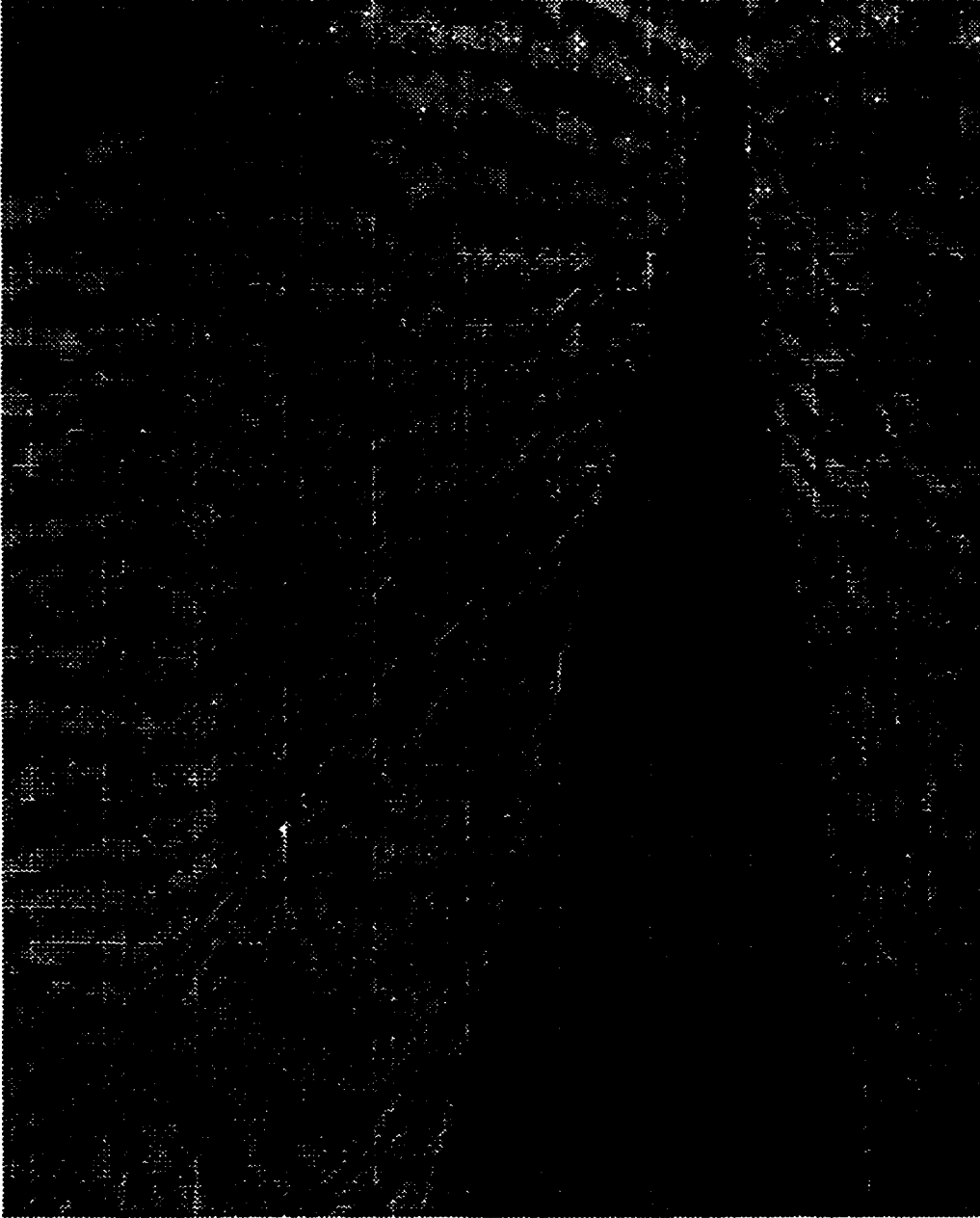


Fig. 36. Finite Fringe Interferogram of Wedge at Mach 3.

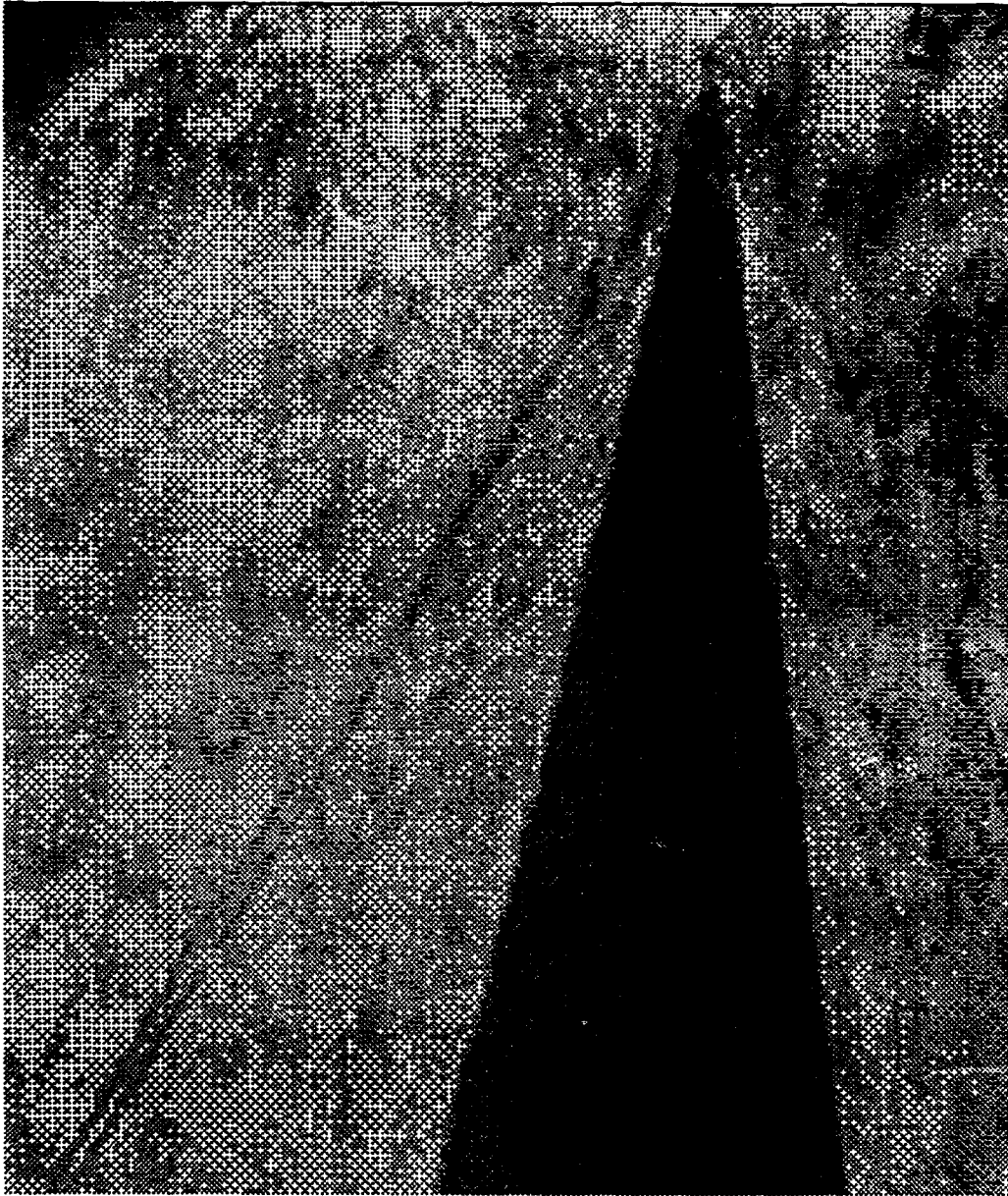


Fig. 37. Shadowgram of Wedge at Mach 3.

6.0 CHEMILUMINESCENCE

For experimental data on high speed vehicles an investigation of aerothermal phenomena in hypersonic flowfields is necessary. However, in low density flows encountered in some hypersonic wind tunnels, diagnostic techniques such as laser velocimetry and interferometry encounter severe handicaps in their application. Thus a diagnostic system based on the chemiluminescent phenomenon has been proposed which may allow improved nonintrusive measurements in low density flowfields. The concept of using a chemiluminescent reaction as a hypersonic diagnostic tool was initially proposed by Aerodyne Products Corporation. The system is currently being developed in the Wright Laboratory for use in the 20-Inch Hypersonic Wind Tunnel (HWT).

To the knowledge of the authors, this is the first time the chemiluminescence phenomenon has been explored for application to aerodynamic testing. Although theoretically feasible, the application has yet to be proven. Much of the work done in the initial conceptual development has employed the available data for the reaction. Unfortunately, it appears that no chemical data are available for the reaction at the very low temperatures (35K) encountered in the HWT. Hence, a major task of developing the chemiluminescence system is measuring the intensity and lifetime of the emitted radiation at low density to generate a set of calibration curves.

In the chemiluminescence system nitric oxide reacts with atomic oxygen to produce nitrogen dioxide and simultaneously release a photon in the visible spectrum (Ref. 31, Ref. 32, Ref. 33).



This reaction has been observed in the upper atmosphere (i.e., space shuttle missions) and under controlled conditions in the laboratory. For application in wind tunnels the nitric oxide will be injected into the flow upstream of the nozzle while an ultra-violet laser pulse is used to dissociate molecular oxygen in the test section. The emitted light from the reaction will be collected and processed by either a photo-multiplier tube (PMT) for quantitative point data or a charge-coupled device (CCD) camera for flow visualization or quantitative velocity field measurements. A schematic of the concept is shown in Fig. 38.

As stated earlier the chemiluminescence system may allow for improved diagnostic capabilities in low density flows. Unfortunately, the system is ineffective at higher densities. Nitric oxide reacts with molecular oxygen as well as atomic oxygen, hence under higher density conditions the majority of the nitric oxide is involved in reactions before it can be useful. Similarly, the ultraviolet laser pulse used to dissociate the oxygen will not propagate a sufficient distance through higher density air.

The chemiluminescence system includes hardware for nitric oxide injection, laser beam delivery and light collection and processing. The entire system will be automated and controlled

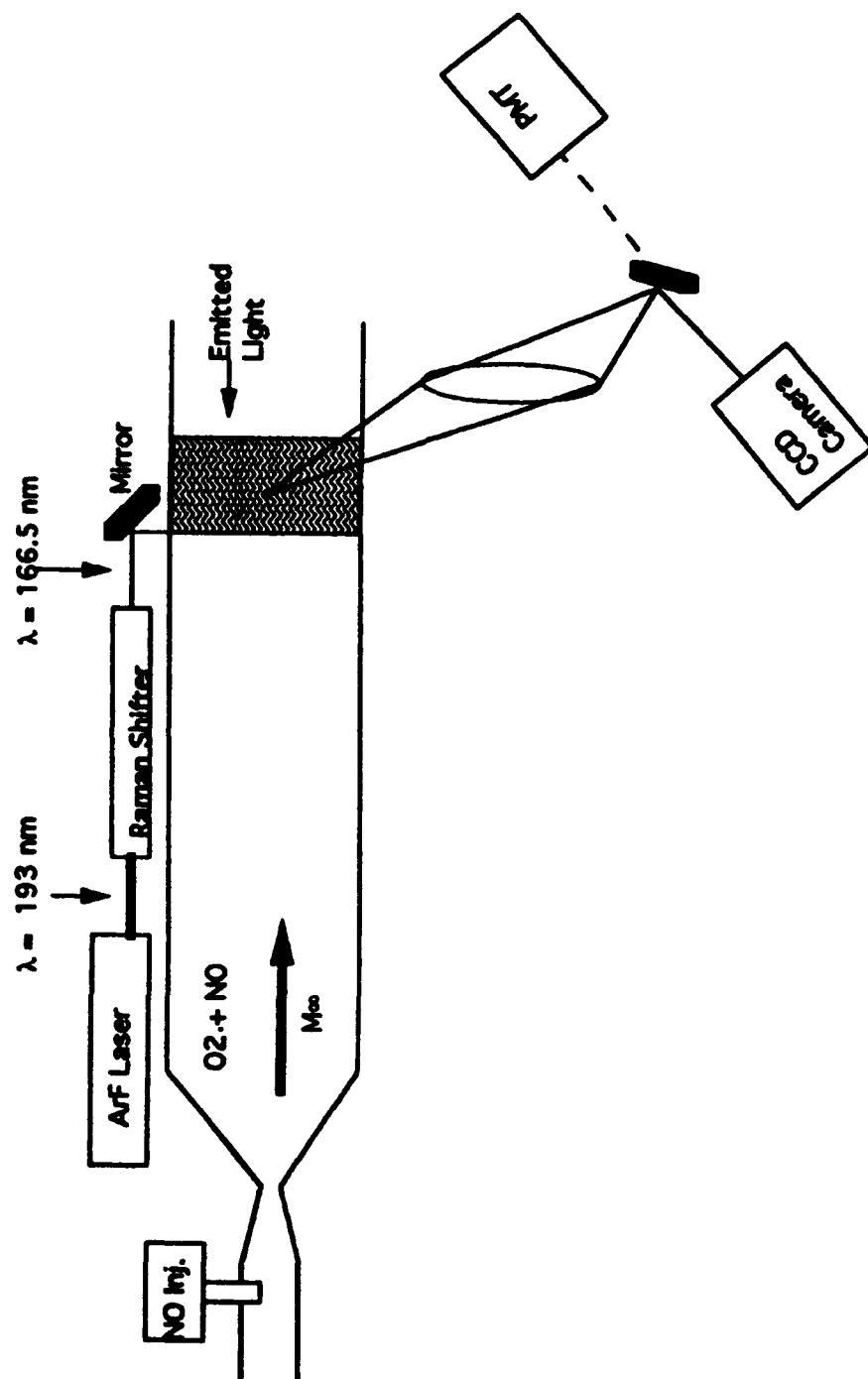


Fig. 38. Chemiluminescence System.

by a microcomputer. The injection system will deliver nitric oxide uniformly across the test section at approximately 1% (0.45 - 0.68 kg/sec) of the tunnel mass flow.

Molecular oxygen in the test section is dissociated by absorption of a photon from the laser at 166.5 nm wavelength. The spectrum of absorption coefficients for molecular oxygen is shown in Fig. 39. The 166.5 nm wavelength was chosen because it contains sufficient energy to dissociate the molecule while having a low enough coefficient of absorption to adequately penetrate the flowfield.

A two stage process is required to produce the 166.5 nm laser pulse. Initially a 193 nm pulse is generated by an ArF excimer laser. The pulse is then passed through a Raman cell which uses the Raman effect (Ref. 34) to shift some of the energy in the pulse to the lower wavelength of 166.5 nm. The Raman cell is a long stainless steel tube filled with hydrogen. The Raman effect occurs when a photon excites a molecule to a higher energy state. The molecule can either relax to the same energy state or a different one. If the molecule relaxes to an energy state other than its initial state, the net change in energy experienced by the molecule is balanced by a change in energy between the exciting and emitted photons. Thus, if the molecule relaxes to a higher energy state the photon loses energy and is emitted at a lower wavelength. Inversely, if the molecule relaxes to a lower energy state the emitted photon leaves at a shorter wavelength with more energy. Noble (Ref. 34) provides a thorough discussion on the Raman effect and Raman cells.

As the chemical reaction occurs in the test section photons are released and the emitted light is captured by the collection optics for analysis. The collection optics consist of a lens, a

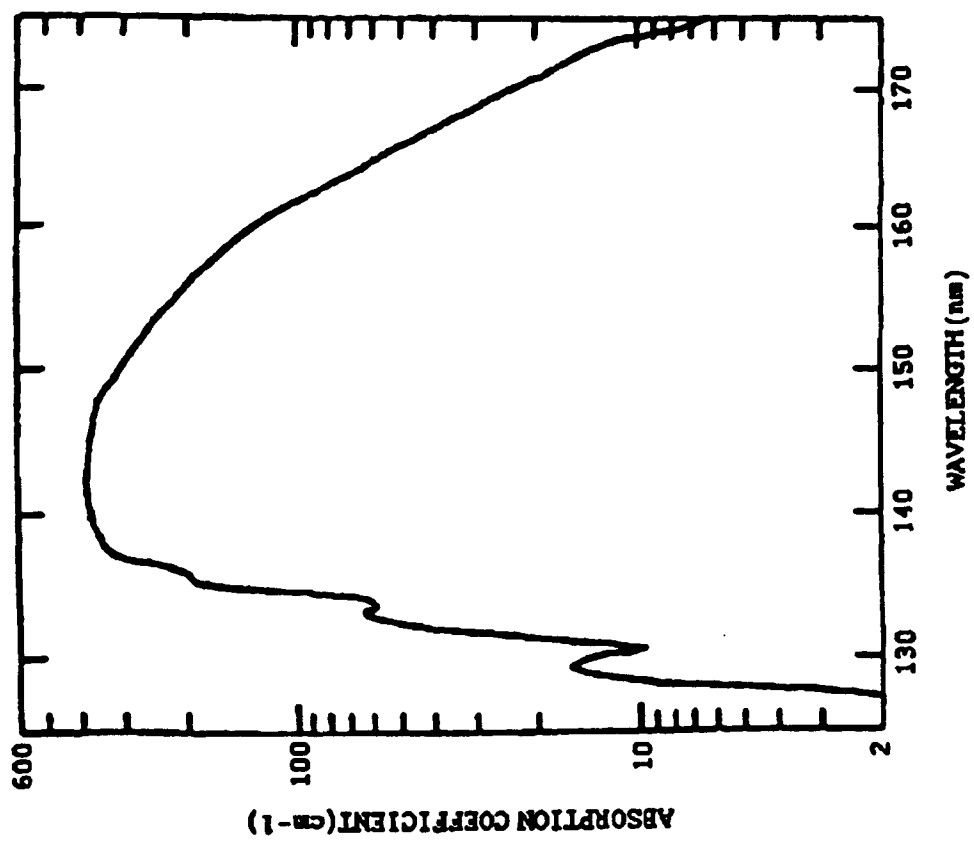


Fig. 39. Spectrum of Absorption Coefficients for Molecular Oxygen.

turning mirror, and either a photo-multiplier tube or a CCD camera. The light is focused through the lens and turned by the mirror into either the PMT or the CCD camera.

Quantitative data are collected by the PMT and then pressure and temperature at a point in the flowfield can be calculated by examining the lifetime and intensity of the emitted light. The complete development of relations to determine temperature, as discussed below, and pressure is given by Camac (Ref. 31). The intensity of the emitted light is given by

$$I = k[NO][O] \quad (26)$$

where I is intensity, k is the intensity rate constant, and the terms in brackets are the number densities of the nitric oxide and atomic oxygen. Using the ideal gas law in terms of number density and assuming k proportional to $T^{-1.55}$ it can be shown that the relation becomes

$$I = k_1 \frac{P^2}{T^{3.55}} \quad (27)$$

where k_1 is a constant, P is the pressure, and T is the temperature of the air. The effective lifetime of the chemiluminescent emission may be expressed as

$$T_{eff} = \frac{1}{K_m n} \quad (28)$$

where K_m is the chemiluminescence rate constant and n is the number density. Assuming the rate constant is proportional to $T^{0.5}$ and using the ideal gas law, the effective lifetime becomes

$$T_{eff} = c \frac{T^{0.5}}{P} \quad (29)$$

where c is a constant. Hence, the intensity and effective emission lifetime are both functions of temperature and pressure. By measuring the emission lifetime and intensity at a known reference condition the temperature and pressure at any other position may be determined from the ratios of the intensity and emission lifetimes. That is

$$T = \left[\frac{T_{eff}}{T_{ref}} \right]^{0.8} \left[\frac{I_{ref}}{I_{usr}} \right]^{0.4} T_{ref} \quad (30)$$

Similar relations can be developed to determine pressure.

Flowfield visualization and velocity field measurements can be made by focusing the emitted light onto a CCD camera. The 40 mm receiving field of the camera combined with the effects of the focusing lens allow a (95.2 square mm) section of the flowfield to be captured by the CCD camera. By initially creating a straight line of dissociated oxygen normal to the flow and using a known camera exposure time the velocity profile of the flow may be determined by examining the length of the emitting region in the picture. Shock waves may also be visualized by examining the change in emission intensity as the flow crosses the shock wave. Sketches of possible flow visualization results are shown in Figs. 40 and 41.

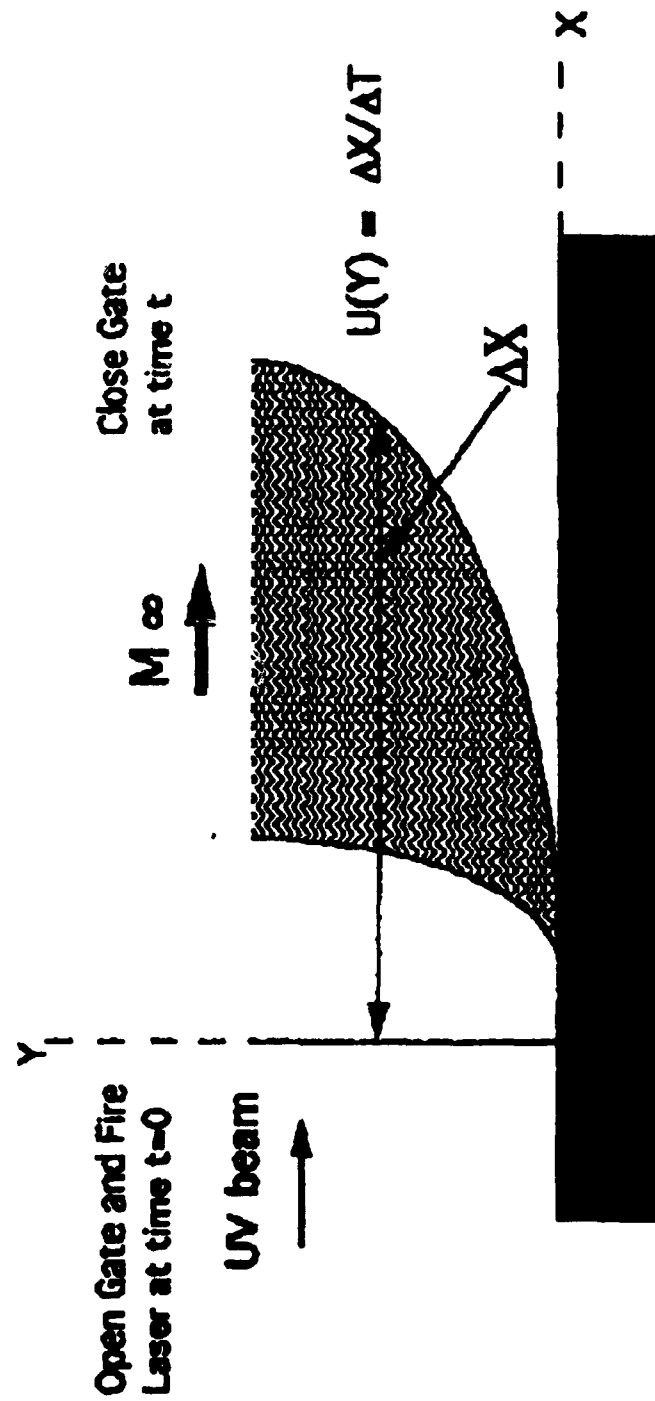


Fig. 40. Velocity Profile from Chemiluminescent Flow Visualization.

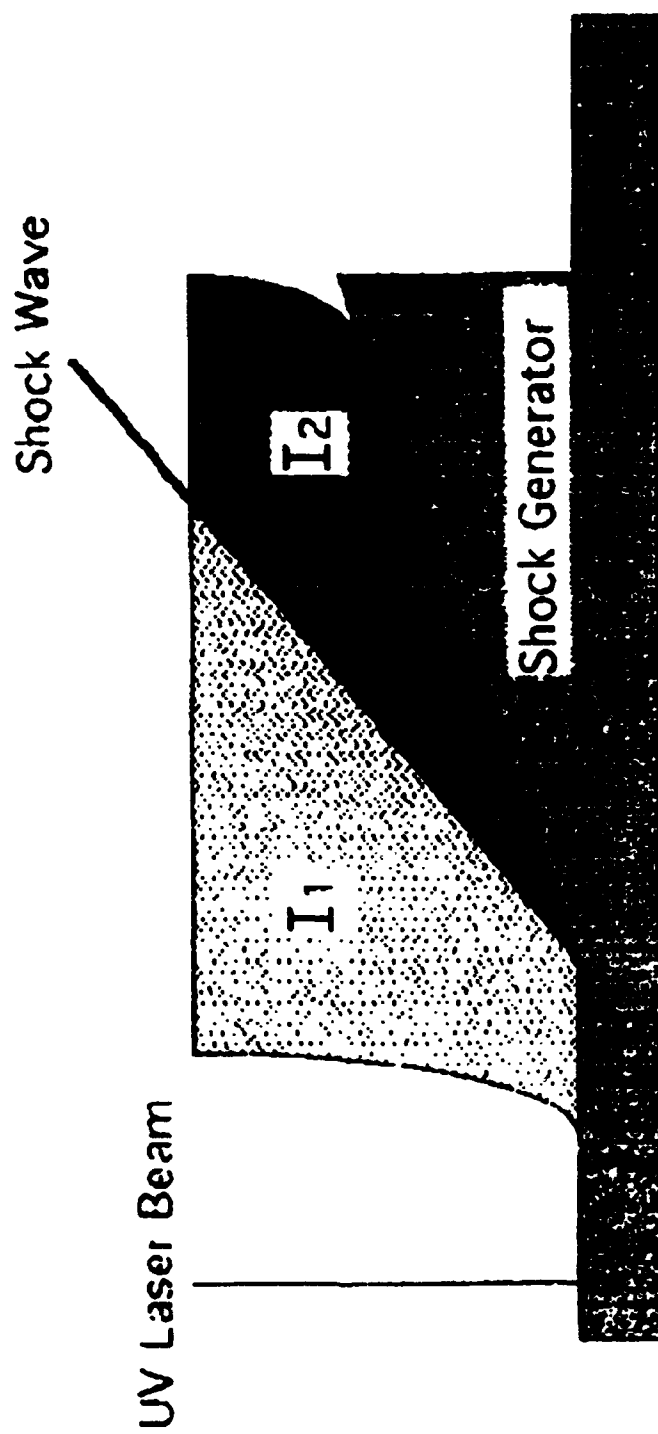


Fig. 41. Example Flow Visualization of Shock Structure Using Chemiluminescence.

The chemiluminescence system is currently being installed for benchtop evaluation. Since many of the chemical reaction rates used in the analysis of the chemiluminescent concept have been extrapolated from higher temperature ranges it is not certain at this time if the concept will work at the very low temperatures encountered in the HWT. A calibration/test cell is being designed to allow for a proof of concept and eventual calibration of the system before it is installed in the hypersonic tunnel.

7.0 OTHER TECHNIQUES

In addition to all of the techniques discussed above, several other systems are worthy of mention. Laser light sheet is a simple technique that has been in use for many years, however, the authors would like to present some of the interesting applications in which this system has provided significant contributions to the overall wind or water tunnel test. Optically smart surfaces is a technique that has been under development at a contractor facility for several years and is expected to be fielded for a wind tunnel test sometime in 1994. Copper vapor light sheet, tomography, and multiple-source schlieren are other techniques which are in the initial development or feasibility study stages. These systems are discussed briefly in the following sections.

7.1 LASER LIGHT SHEET

A thin planar sheet of laser light, generated with an argon laser by expanding the beam with a cylindrical glass rod, is used to illuminate a cross-section of the flowfield for video or photographic recording. For the Large Water Tunnel (2 ft. square) the light sheet is positioned by mounting a 4-Watt laser and optics on a heavy duty tripod with manual elevation adjustments and rotational capabilities on a glass rod and a mirror. Using this control system the light sheet can be manually manipulated to provide cross-sectional views of the flowfield that are normal to the model or any other configuration desired by the test engineer. The width of the light sheet is controlled by the diameter of the glass rod. In the large water tunnel, a fluorescent dye is pumped out of model pressure ports such that the dye is trapped in the flow structure under

investigation. The fluorescent dyes give off orange or yellow light when excited with the green light of the argon laser. This technique is ideal for qualitative studies of vortex structures or boundary layer profiles.

In the Mach 6 HRNF, a 15-Watt argon laser is positioned on the LV traversing table and the beam is expanded using a cylindrical glass rod or a cylindrical lens. Silicon oil is used for seeding the flowfield. This light sheet system has been used to study flow patterns for determining the grid for LV data points and for locating shock waves inside the P-8 inlet model. It has also been used for analysis of the seeding pattern to determine regions of the flowfield which are not suitably seeded for LV measurements.

In the TGF, a 4 or 15-Watt argon laser is used on one of the traversing systems mentioned above, or by using a fiber optic system for easier traversing. For the fiber optic system, the cone of light exiting the fiber cable is focused with a 50 mm diameter, 150 mm focal length lens and expanded into a sheet with a 75 or 150 mm focal length cylindrical lens. The head containing the sheet forming optics is mounted on a tripod. Seeding of the freestream flow in the TGF is accomplished by running the tunnel without the dryers and by injecting water vapor in the stagnation chamber in sufficient quantities to produce a fog in the test section. The light sheet has been used to study flow patterns prior to doing LV work, vortex flows at subsonic and supersonic speeds, vortex bursting using high speed video, vortex control on an X-29 forebody model, shock waves in a supersonic boundary-layer controlled inlet model, and jet exhaust from a nozzle model.

Light sheet visualization is done in the SARL using the same fiber optic system described for the TGF, except the head is mounted on a traverse on top of the test cabin. Flow seeding has been done with smoke generated vaporizing oil or commercial smoke fluids, water spray, and natural condensation. This system can output 4.5 Watts of laser light and has been used to study vortex flows about a model rolling at 8 Hz about the pitch axis with high speed video, vortex flows on swept wing models, flow patterns about a Maverick ring wing missile, and flow out of a model simulating an airliner cabin decompression after a bomb explosion.

7.2 COPPER VAPOR LIGHT SHEET

A copper vapor laser has been acquired for use in a pulsed light sheet visualization system. The copper vapor laser light will be spread into a thin sheet of light similar to that described in the section on laser light sheet above and used to capture images of unsteady flowfields. The copper vapor laser pulses at 9-12 kHz with pulse durations on the order of 10 nsec and power levels near 15 W per pulse. Thus this pulsed laser light sheet will be ideal for capturing unsteady flowfield cross-sections of oscillating airfoils or of turbulent structures in a supersonic boundary layer. A high-speed personal computer and frame grabber with graphics software is being acquired for the task. Initial testing is expected to take place in summer 1993, with a study of the boundary layer on the test section floor of the Mach 3 HRNF.

7.3 OPTICALLY SMART SURFACES

Optically smart surfaces is a program in the developmental stage, which shows tremendous potential. The proof of concept research has concluded that holographic optical

elements can be used for velocity and coupled strain/temperature measurements in a laboratory setting (Ref. 35). Initial testing shows that a laser velocimetry probe volume can be created and doppler signal produced with seed particles.

In the case of a holographic sensor that produces a laser doppler probe volume, the image of a probe volume generated by intersecting laser beams is stored in a hologram on the surface of the model. When this hologram is addressed by a laser beam, the probe volume is reconstructed within the flow. This method of generating probe volumes will allow the experimenter to make laser velocimetry measurements in forward scatter at locations on the model where traditional forward scatter measurements are impossible because of model interference. The optical theory of this method is given by Trolinger and Rosenthal (Ref. 35).

Holographic sensors can also be used for measuring temperature and surface strain. Thermal expansion or mechanical stresses cause a diffracted beam to modulate in a measurable way. Again, the theory of the optical modulation is given by Trolinger and Rosenthal (Ref. 35). The difficulty with this method at the current time is that the effects of temperature and strain are coupled and a method for discriminating temperature and strain effects has not yet been developed.

Additional research in the development of optically smart surfaces for an environment harsher than a clean laboratory is ongoing at the contractor's facility. After initial development of a ruggedized holographic sensor, it will be tested in a low-speed subsonic wind tunnel. Following further design analysis of the ruggedized holographic sensors, they will be tested in the Trisonic Gasdynamics Facility.

7.4 TOMOGRAPHY

Interferometry is limited to two-dimensional or axisymmetric flowfields, but many flowfields of interest are three-dimensional. Tomography is a variation of interferometry that uses slices of the flowfield and large computer reconstruction techniques to develop three-dimensional results. Cha (Ref. 36) evaluated the existing wind tunnels in the Aeromechanics Division for the feasibility of applying tomography to the facility. The results of his evaluation are shown in Table II. Further development of reconstruction techniques are underway by Cha.

Table 2: Feasibility of Tomography in Facilities

Facility	Evaluation Results
M3 HRNF	Application recommended
M6 HRNF	Application recommended
TGF (Supersonic)	Skeptical
TGF (Transonic)	Further study required
TGF (Subsonic)	Further study required
HWT	Further study required
SARL	Not recommended

7.5 MULTIPLE-SOURCE SCHLIEREN

The schlieren has long been a popular and useful tool for nonintrusive visualization of flowfields. However, due to the integration property of schlieren, density gradients external to the flowfield of interest, but within the optical path, may significantly increase the noise present in the system. These external gradients may be due to any number of sources, including thermal currents within the room or turbulent boundary layers on test section windows. The resulting external interference may be of sufficient strength to render the system useless, especially in the case of very low density flows where changes in density external to the flowfield may be of the same order as changes of density within the flowfield. In an effort to develop schlieren systems which alleviate the detrimental affects of external noise, the Aero-Diagnostics Research Section is supporting the work of Dr. Steven Collicott of Purdue University in the development of multiple-source (or focus) schlieren systems (Ref. 37).

Although both coherent and incoherent light sources may be used to drive a multiple-source schlieren system, the system employing the incoherent light source is the simplest to understand. The following discussion assumes the reader is familiar with the operating principles of a standard schlieren system.

Operating from an incoherent light source, a multiple-source schlieren system uses a series of source slits each with its own knife edge, as opposed to the single source and knife edge of a traditional system. Each source/slit combination acts as a single schlieren system with the image produced by each system superimposed on the image plane. The centerlines of all the sub-systems are coincident at the ideal object and image planes. Away from these planes the

centerline of each system is not coincident with the other systems. Thus, the image of the object plane generated by each subsystem is superimposed with the image generated by the other subsystems and the object plane image is "built-up" on the image surface. Images of the regions outside the object plane are not coincident in the image plane and tend to be dispersed into the background.

8.0 CONCLUSIONS

Laser velocimetry, laser induced fluorescence, Rayleigh scattering, phase shift holographic interferometry, and chemiluminescence are some of the new advanced laser-based diagnostics techniques being developed and applied in the Aeromechanics Division. The results of wind tunnel test measurements made with these systems will contribute to a quality database of aerodynamic data for hypersonic vehicle design and CFD validation. These systems provide techniques for measurement of temperature, pressure, density, velocity, and surface strain.

The state of the art in laser velocimetry applications has been advanced several times by the Aero-Diagnostics Research Section in the past 5 years. Additional research into the application of this technique and particle bias analysis for CFD code validation will continue. The primary focus of the LV system has been the Mach 3 HRNF, Mach 6 HRNF, TGF, and HWT although some testing has been conducted in the water tunnel and SARL.

The laser induced fluorescence and Rayleigh scattering systems will measure temperature and density at a point location by measuring the light fluoresced and/or scattered from oxygen molecules. These systems are currently being developed for use in the Mach 6 high Reynolds number facility with transition to the Mach 3 high Reynolds number facility expected at a later time. Quantitative data have been collected with errors near 40%, but research is being conducted to identify and correct for the measurement biases.

The phase shift holographic interferometry system measures the index of refraction of the air in the wind tunnel. From the index of refraction, the density of a two-dimensional or axisymmetric flowfield may be calculated. The phase shift holographic interferometry system can be used in the Mach 3 and Mach 6 High Reynolds Number Facilities and the Trisonic Gasdynamics Facility. Data reduction software is currently being developed.

The chemiluminescence system will measure the intensity and effective lifetime of the light emitted by the chemiluminescence reaction. From this data, the temperature and pressure of a point in the flow may be calculated. Or, using a CCD camera, this technique may be used for flow visualization or quantitative velocity field measurements. A calibration test cell is currently being developed so that the reaction rate coefficients may be determined in a controlled environment. This system will be installed in the 20-Inch Hypersonic Wind Tunnel.

Laser light sheet provides a good cross-sectional view of the flowfield and assists the test engineer in optimizing other measurements. The copper vapor light sheet will extend the light sheet concept to unsteady flowfields and capturing the cross-sections in a short pulse duration. Optically smart surfaces will provide an alternative method for obtaining laser velocimetry or strain measurements. Tomography, multiple-source schlieren, and doppler global velocimetry are techniques with great futures, but they are in the infancy stage of development in the Aeromechanics Division.

Overall, the new advanced diagnostics techniques under development look to be very promising as new methods of nonintrusive measurements. Added to the current state-of-the-art

capabilities of the laser velocimetry system, these techniques should help to generate a complete database of aerodynamic data for hypersonic vehicle design and CFD validation.

9.0 REFERENCES

1. Hirai, E., Bütefisch, K.A. and Dankert, C., Apr 1992, "Velocity and Density Determination by the Electron Beam Technique," New Trends in Instrumentation For Hypersonic Research, NATO Advanced Research Workshop, Paper 5D, ONERA, LeFauga - Maizac, France.
2. Palmer, J.L., McMillin, B.K. and Hanson, R.K., Jan 1992, "Planer Laser-Induced Fluorescence Imaging of Velocity and Temperature in Shock Tunnel Free Jet Flow," AIAA Paper 92-0762.
3. Miles, R.B., Lempert, W.R. and Forkey, J., Jan 1991, "Instantaneous Velocity Fields and Background Suppression by Filtered Rayleigh Scattering," AIAA Paper 91-0357.
4. Smith, L.G., Tyler, C., and Schmisser, J.D., Oct 1992, "Advanced Diagnostics Research for High Speed Aerodynamic Testing," SAE Paper 922007.
5. Watrasiewicz, B.M. and Rudd, M.J., 1976, Laser Doppler Measurements, Butterworths & Co, Boston, MA.
6. Molezzi, M.J. and Dutton, J.C., Jan 1992, "Development and Application of a Particle Image Velocimeter For High-Speed Flows," AIAA Paper 92-0004.

7. Komine, H., Brosnan, S.J. and Litton, A.B., Jan 1991, "Real-Time Doppler Global Velocimetry," AIAA Paper 91-0337.
8. Menon, R. and Lai, W.T., Aug 1991, "Key Considerations in the Selection of Seed Particles For LDV Measurements," Laser Anemometry - Advances and Applications, Vol. 2, ASME, New York, NY, pp. 719-730.
9. Rudoff, R.C. and Bachalo, W.D., Aug 1991, "Seed Particle Response and Size Characterization in High Speed Flows," Laser Anemometry - Advances and Applications, Vol. 2, ASME, New York, NY, pp. 443-448.
10. Maurice, M.S., Jan 1992, "A Method to Quantify and Correct Particle Velocity Bias in Laser Velocimetry Measurements," AIAA Paper No. 92-0764.
11. Seibert, G.L., Maurice, M.S., and Scaggs, N., "Turbulence Production Over a Rough Wall at Mach 3," FED-Vol. 55, Third International Symposium on Laser Anemometry, The Winter Annual Meeting of ASME, Boston, MA, December 1987, pp 101-107.
12. Maurice, M.S. and Seibert, G.L., Jul 1989, "The LV Measured Turbulent Structure of Mach 6 Flow over a Roughened Flat Plate with a Compression Ramp," AIAA Paper No. 89-2164-CP.

13. Smith, L.G., Maurice, M.S., Seibert, G.L., and Tyler, C., Jun 1991, "Laser Velocimetry Measurements of Supersonic Vortex Flows on a Simple Razor-Edged Delta Wing," AIAA Paper No. 91-1684.
14. Maurice, M.S., Feb 1992, "Laser Velocimetry Seed Particles Within Compressible, Vortical Flows," AIAA Journal, Vol. 30, No. 2, pp. 376-383.
15. Webster, W.P. and Shang, J.S., Jan 1990, "Comparison Between Thin Layer and Full Navier-Stokes Simulations Over a Supersonic Delta Wing," AIAA Paper 90-0589.
16. Crowe, C.T., May 1967, "Drag Coefficient of Particles in a Rocket Nozzle," AIAA Journal, Vol. 5, No. 5, pp. 1021-1022.
17. Maurice, M.S., Jun 1991, "The Effect of High Speed Expansion Turns on LV Measurement Bias," FED-Vol. 108, Fluid Measurement and Instrumentation Forum, First ASME/JSME Fluids Engineering Conference, pp 83-88.
18. Maurice, M.S., Jan 1993, "Quantitative Laser Velocimetry Measurements in the Hypersonic Regime by the Integration of Experimental and Computational Analysis," AIAA Paper 93-0089.
19. Maurice, M.S., Jul 1992, "A Particle Size Distribution Technique Using Conventional Laser Velocimetry Measurements," AIAA Paper 92-3896.

20. Schmisser, J.D., Wagner, M., Maurice, M.S., Miller, C.D. and Barber, C.T., "Assessment of Laser Velocimetry Within the Flight Dynamics Directorate 20 Inch Hypersonic Wind Tunnel," Wright Laboratory Technical Report, WL-TR-93-3067, July 1993.
21. O'Keefe, A., May 1992, "Hypersonic Flow Diagnostics Development," Final Report, Wright Laboratory WL-TR-92-3034, Wright-Patterson AFB, OH.
22. Shirinzadeh, B., Hillard, M.E., and Exton, R.J., "Condensation Effects on Rayleigh Scattering Measurements in a Supersonic Wind Tunnel," AIAA Journal, Vol. 29, No. 2, pp. 242-246, February 1990.
23. Shirinzadeh, B., Hillard, M.E., Blair, A.B., and Exton, R.J., Jun 1992, "Study of Cluster Formation and its Effects on Rayleigh and Raman Scattering Measurements in a Mach 6 Wind Tunnel," AIAA Paper No. 91-1496.
24. Havener, A.G., and Kirby, D., Jan 1992, "Aero-Optical Phase Measurements Using Fourier Transform Holographic Interferometry," AIAA Paper No. 92-0379.
25. Carré, P., 1966, "Installation et utilisation du comparateur photoélectrique et interférentiel du Bureau International des Poids et Mesures," Metrologia 2, p. 13.
26. Bruning, J.H. et al., Nov 1974, "Digital Wavefront Measuring Interferometer for Testing Optical Surfaces and Lenses," Applied Optics, Vol. 13, No. 11, pp. 2693-2703.

27. Creath, K., 1988, "Phase-Measurement Interferometry Techniques," Progress in Optics Volume XVI, Elsevier Science Publishers, pp. 349-393.
28. Spring, W.C., Yanta, W.J., Gross, K. and Lopez, C.A, Apr 1992, "The Use of Holographic Interferometry for Flow Field Diagnostics," Proceedings of the NATO Advanced Research Workshop, "New Trends in Instrumentation for Hypersonic Research."
29. Vest, C.M., 1979, Holographic Interferometry, John Wiley & Sons, p. 344.
30. Bracewell, R.N., 1986, The Fourier Transform and Its Applications, 2nd Edition, Revised, McGraw-Hill Publishing Company, pp. 262-266.
31. Camac, M., 1992, "Supersonic Flowfield Measurements with NO₂ Chemiluminescent Radiation," Final Report to Wright-Patterson AFB, OH.
32. Baulch, D.L., Drysdale, D.D., Horne, D.G., and Lloyd, A.G., 1993, Evaluated Kinetic Data for High Temperature Reactions, Vol 2., Butterworths, London.
33. Kaufman, F., 1973, "The Air Afterglow Revisited," Chemiluminescence and Bioluminescence, edited by Cormier, M.J., Hercules, D.M., and Lees, J., Plenum Press, NY.
34. Noble, M., Nov 1991, "Reaching Those Awkward Wavelengths," Lasers and Optonics, Vol. 10.

35. Trolinger, J.D., and Rosenthal, D.M., Jul 1992, "Optically Smart Surfaces for Aerodynamic Measurements," AIAA Paper No. 92-3895.
36. Cha, S.S., Aug 1991, "A Study of Optical Methods for High-Speed Aerodynamic Testing at Wright Laboratory," Air Force Office of Scientific Research Final Report for Summer Faculty Research Program.
37. Collicott, S.H., Oct 1992, "Determination of Multiple-Source Schlieren System Capabilities," Final Report for Air Force Office of Scientific Research Summer Faculty Research Program.
38. Parobek, D.M., Boyer, D.L. and Clinehens, G.A., "Recent Developments in Liquid Flow Seeding Techniques for use with LV Measurements," AIAA Paper No. 86-0769, March 1986.